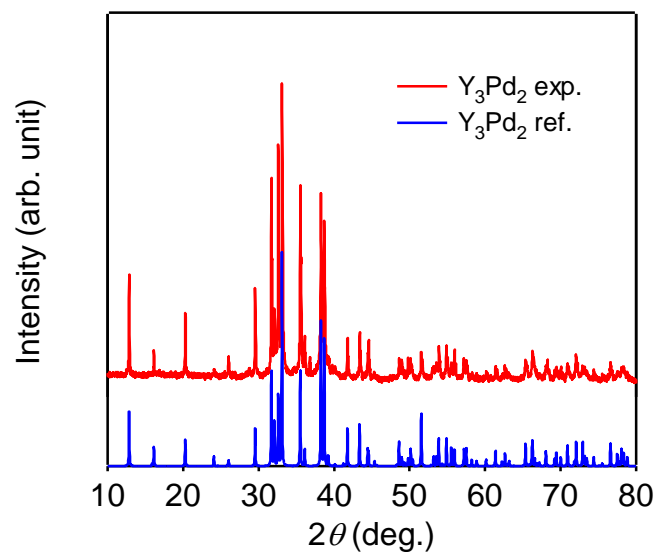


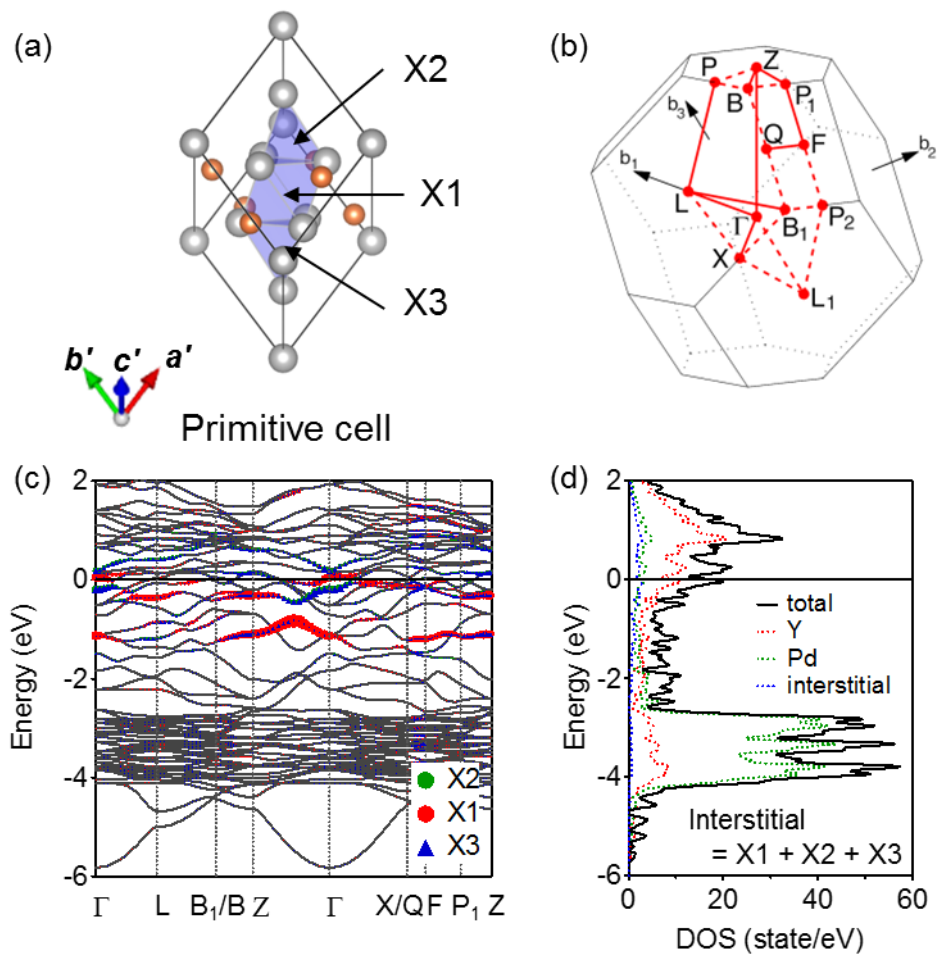
Supplementary Information

**Palladium-bearing intermetallic electride as efficient
and stable catalyst for Suzuki cross-coupling reactions**

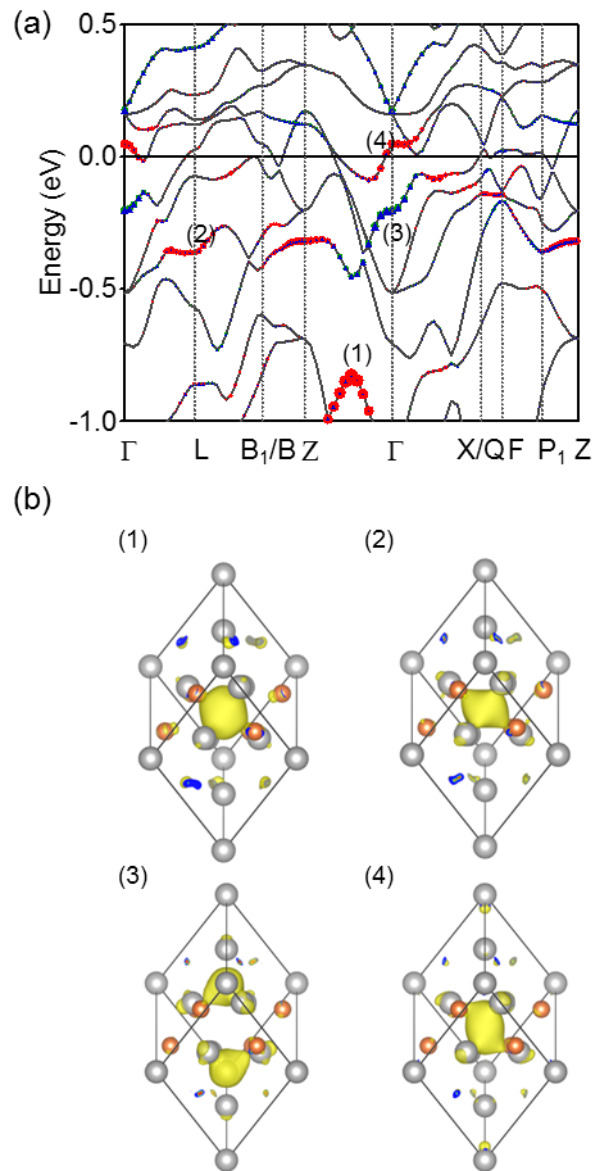
Ye et al.



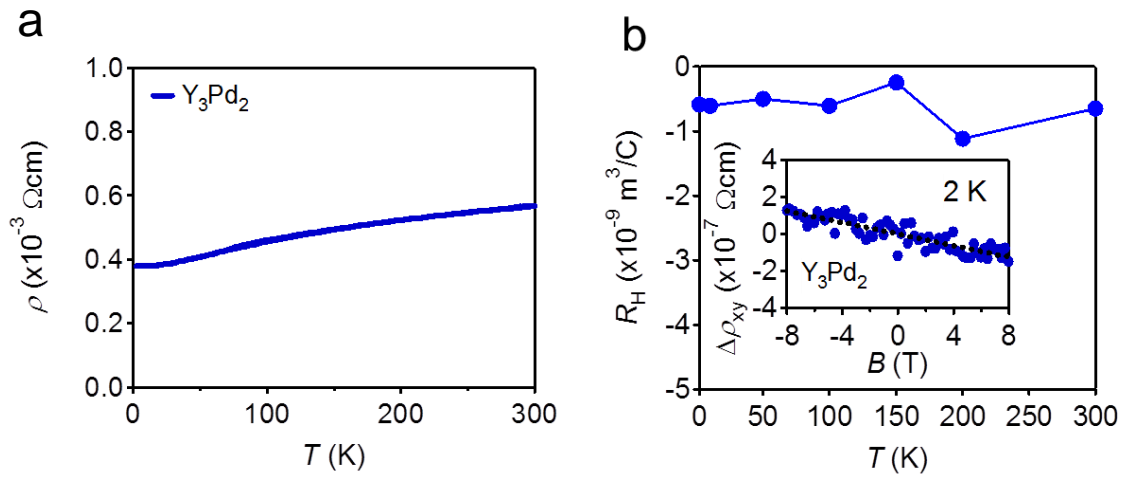
Supplementary Figure 1 | Powder XRD pattern of Y_3Pd_2 . The powder XRD pattern of the as-prepared Y_3Pd_2 . The red and blue solid lines represent experimentally obtained and calculated pattern.



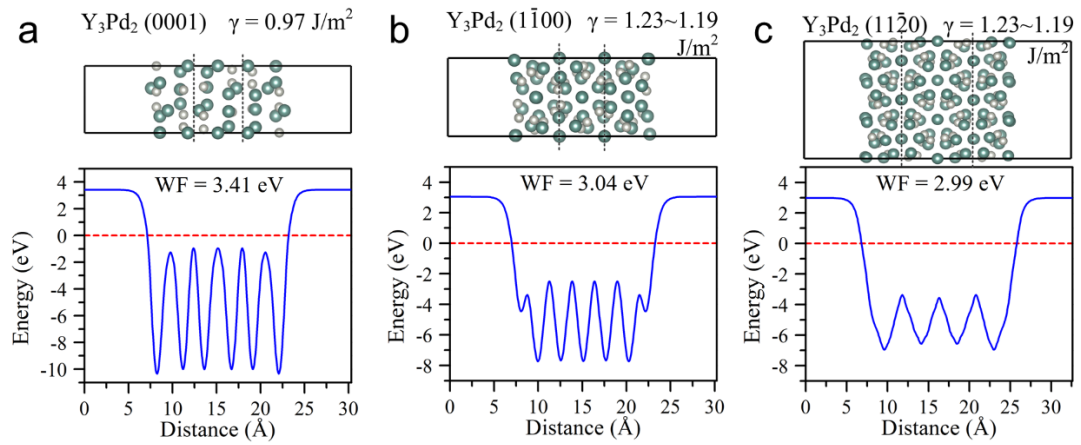
Supplementary Figure 2 | Calculated electronic structure of Y_3Pd_2 . (a) Crystal structure (Primitive cell) of Y_3Pd_2 and (b) The geometry of the first Brillouin zones of Y_3Pd_2 based on the primitive cell. (c) Electronic band structure, and (c) DOSs for the stoichiometric Y_3Pd_2 . The contribution of X1, X2 and X3 sites are emphasized using red, green and blue dots in (c).



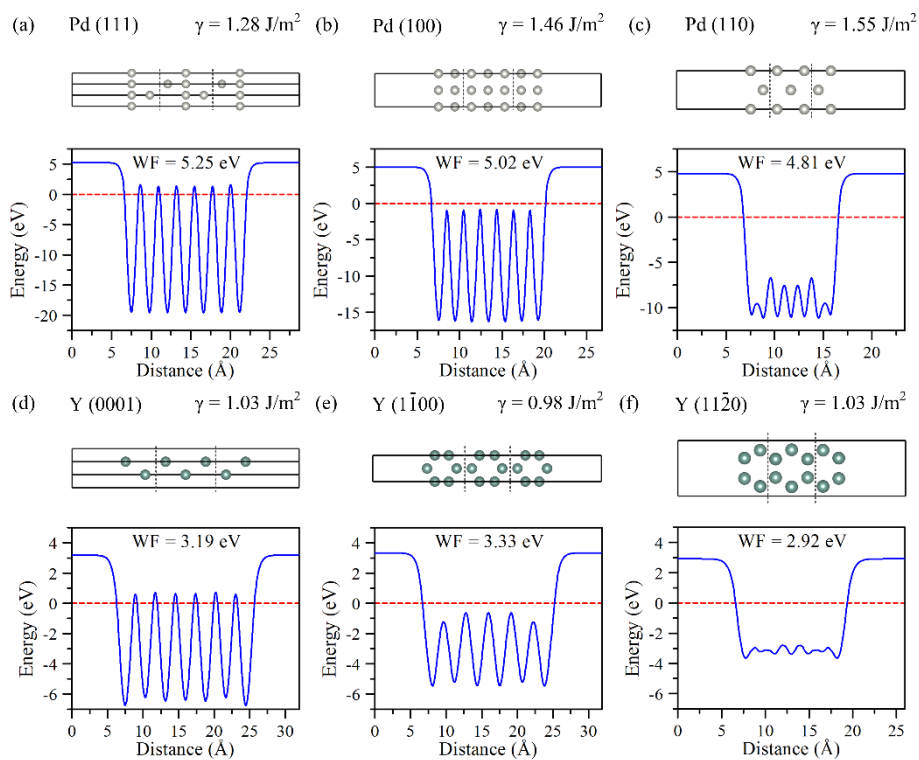
Supplementary Figure 3 (a) The calculated electronic structure of Y_3Pd_2 with narrower energy range. The contribution of X1, X2 and X3 sites are emphasized using red, green and blue dots. (b) Real space electron distribution at corresponding energy bands.



Supplementary Figure 4 | Physical properties of Y_3Pd_2 . a, Electrical resistivity and b, Hall coefficient of Y_3Pd_2 . The inset of represents Hall resistivity measured at 2 K.

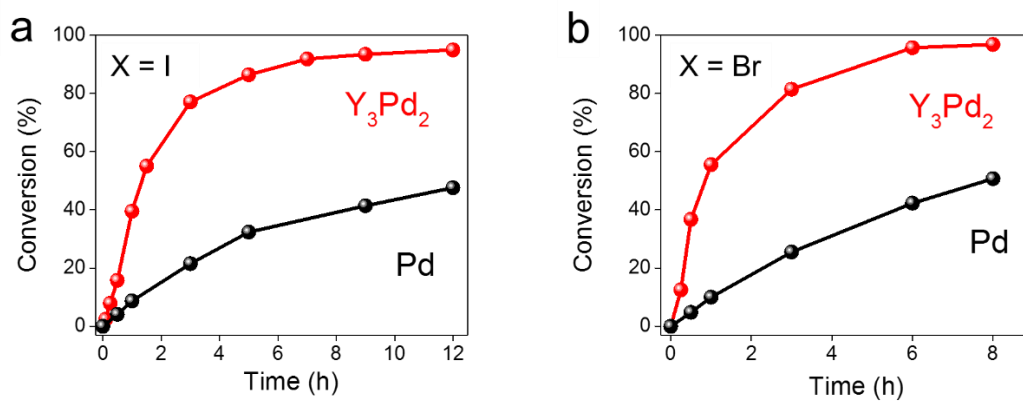
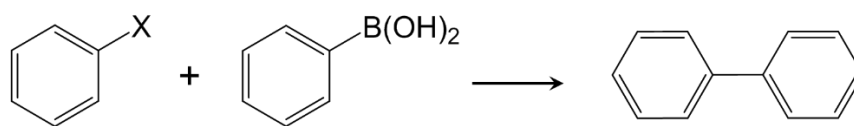


Supplementary Figure 5 | Calculated work functions of Y_3Pd_2 . The corresponding slab models and surface energies are also given. The red dashed lines indicate the Fermi levels.

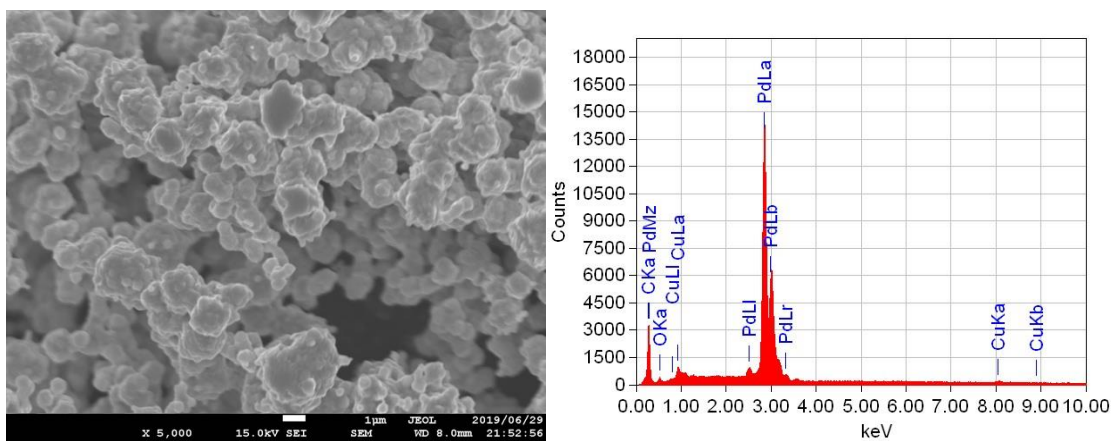


Supplementary Figure 6 | Calculated work functions of different surfaces of Y and Pd metal.

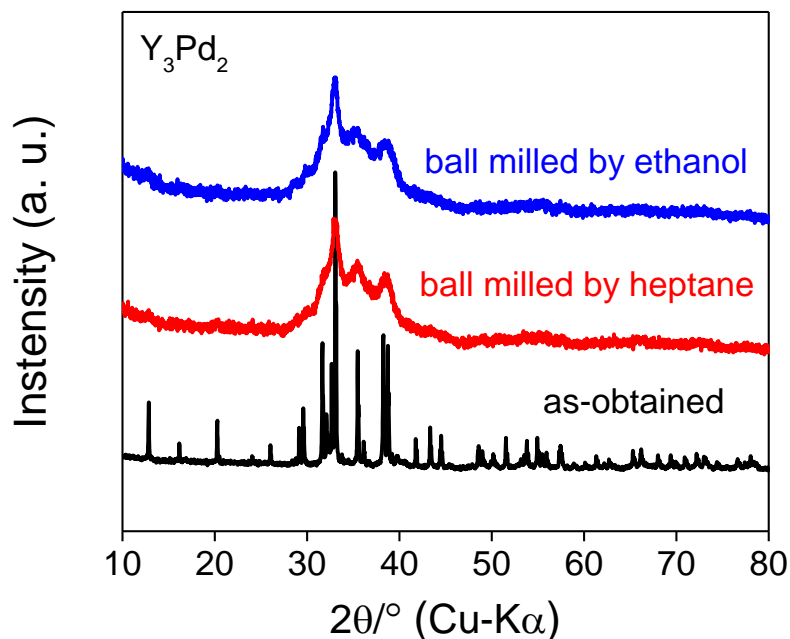
The corresponding slab models and surface energies are also given. The red dashed lines indicate the Fermi levels.



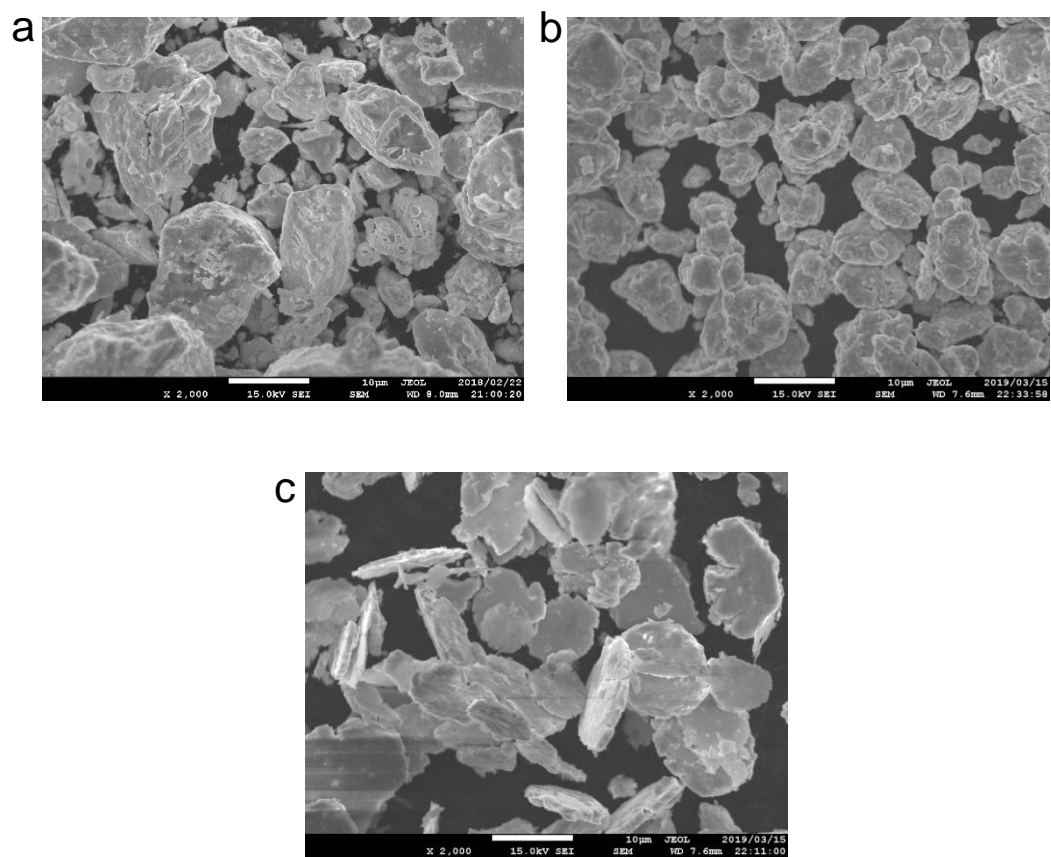
Supplementary Figure 7 Time-dependent catalysis over Y₃Pd₂ and pure Pd metal catalysts for Suzuki coupling reaction of iodobenzene and bromobenzene with phenylboronic acid. Reaction conditions: Pd (40 mol% relative to organohalide); 0.5 mmol organohalide, 0.8 mmol phenylboronic acid, 1.5 mmol K₂CO₃, 5ml solvent, iodides 30°C, bromides 60°C.



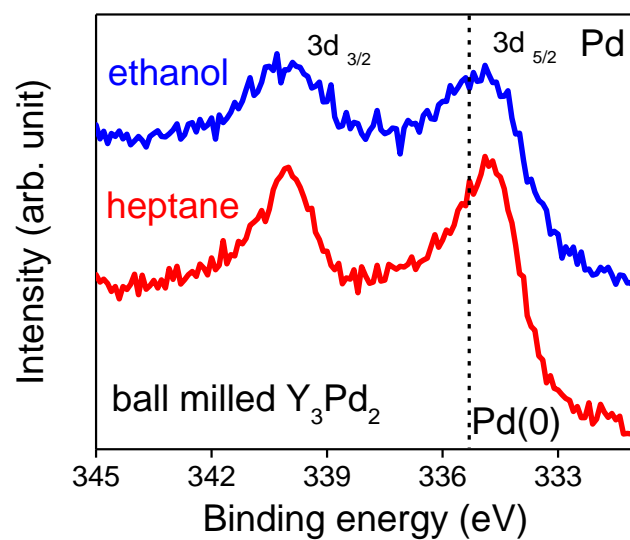
Supplementary Figure 8 | The SEM images and EDS spectra of the reference pure Pd. The signals of C and Cu are derived from carbon paste and sample holder (brass), respectively. And the tiny O species should be the adsorbed oxygen molecule due to the exposure to the air of Pd sample.



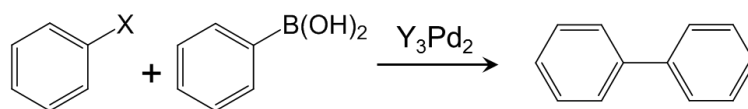
Supplementary Figure 9 | Powder XRD pattern of ball-milled Y_3Pd_2 . The powder XRD pattern of the as-prepared Y_3Pd_2 and ball-milled Y_3Pd_2 in heptane and ethanol respectively. Impurity phases could not be observed in the XRD patterns of both ball-milled samples compared with the as-prepared one. Ball millings were conducted under an Ar atmosphere with heptane or ethanol. The rotation speeds were set to 250 rpm for each and milled for 10 minutes with 10-minute intervals for cooling. This cycle was repeated 20 times. Despite the peaks becoming broader after ball milling, the main peaks still can be identified in these XRD patterns.



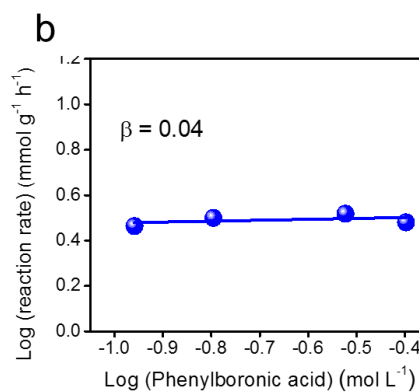
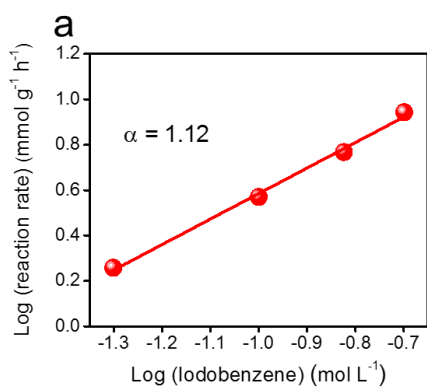
Supplementary Figure 10 The SEM images of the (a) as-prepared Y_3Pd_2 and ball-milled Y_3Pd_2 in (b) heptane and (c) ethanol respectively.



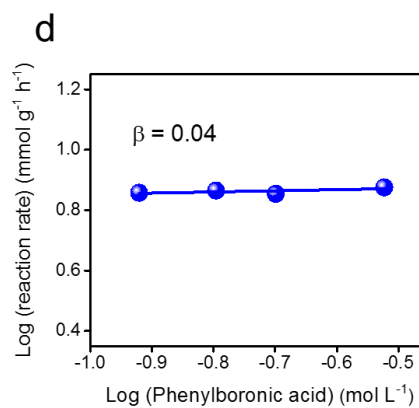
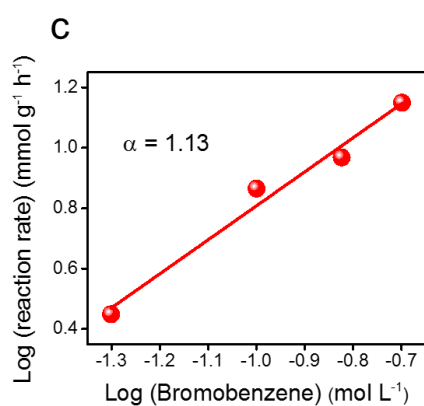
Supplementary Figure 11 XPS Pd 3d spectra for ball-milled Y₃Pd₂ in heptane and ethanol respectively. The XPS measurements revealed obvious red shifts of typical Pd 3d peaks, indicating the Pd active sites in these compounds were negative charged.



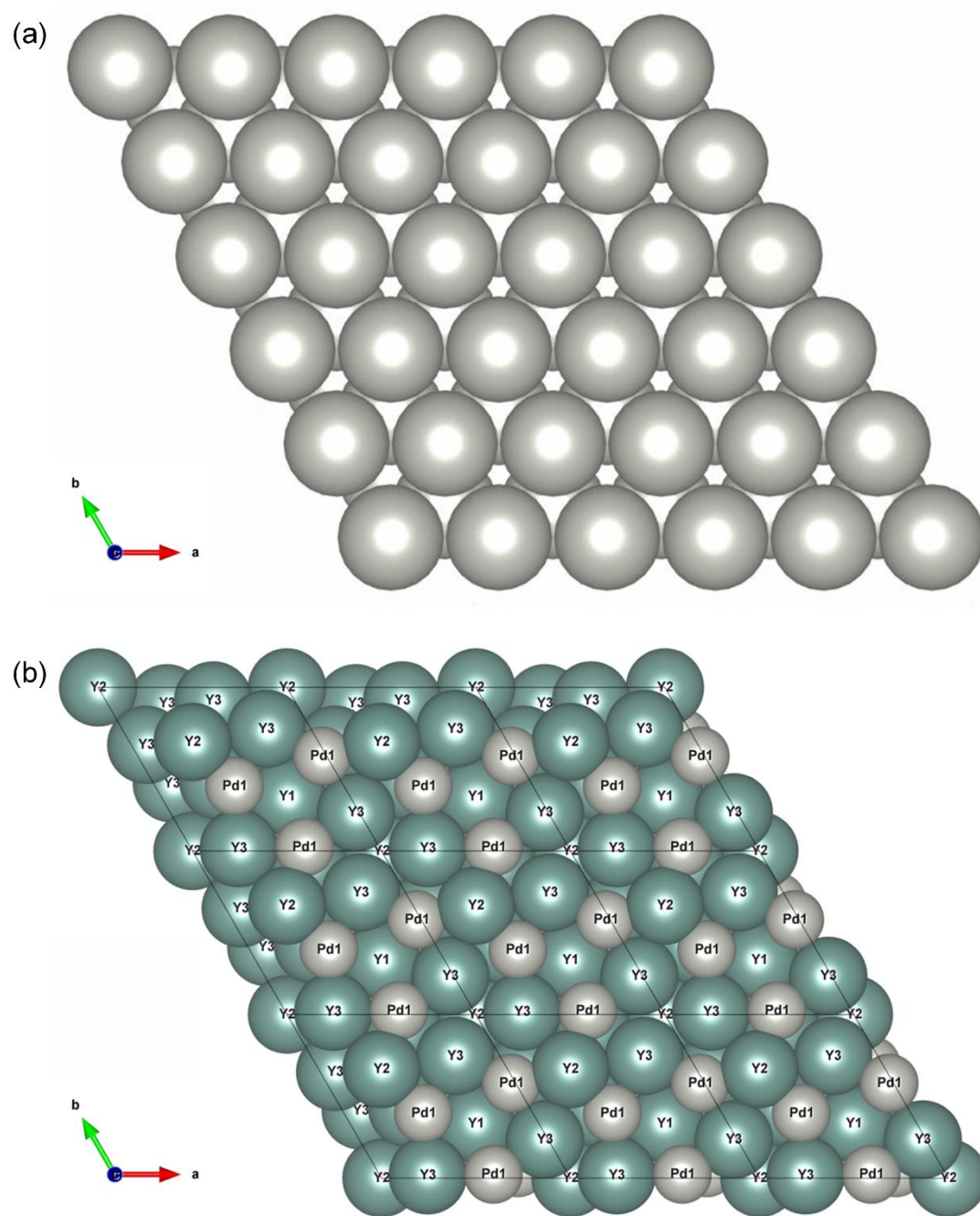
X = I



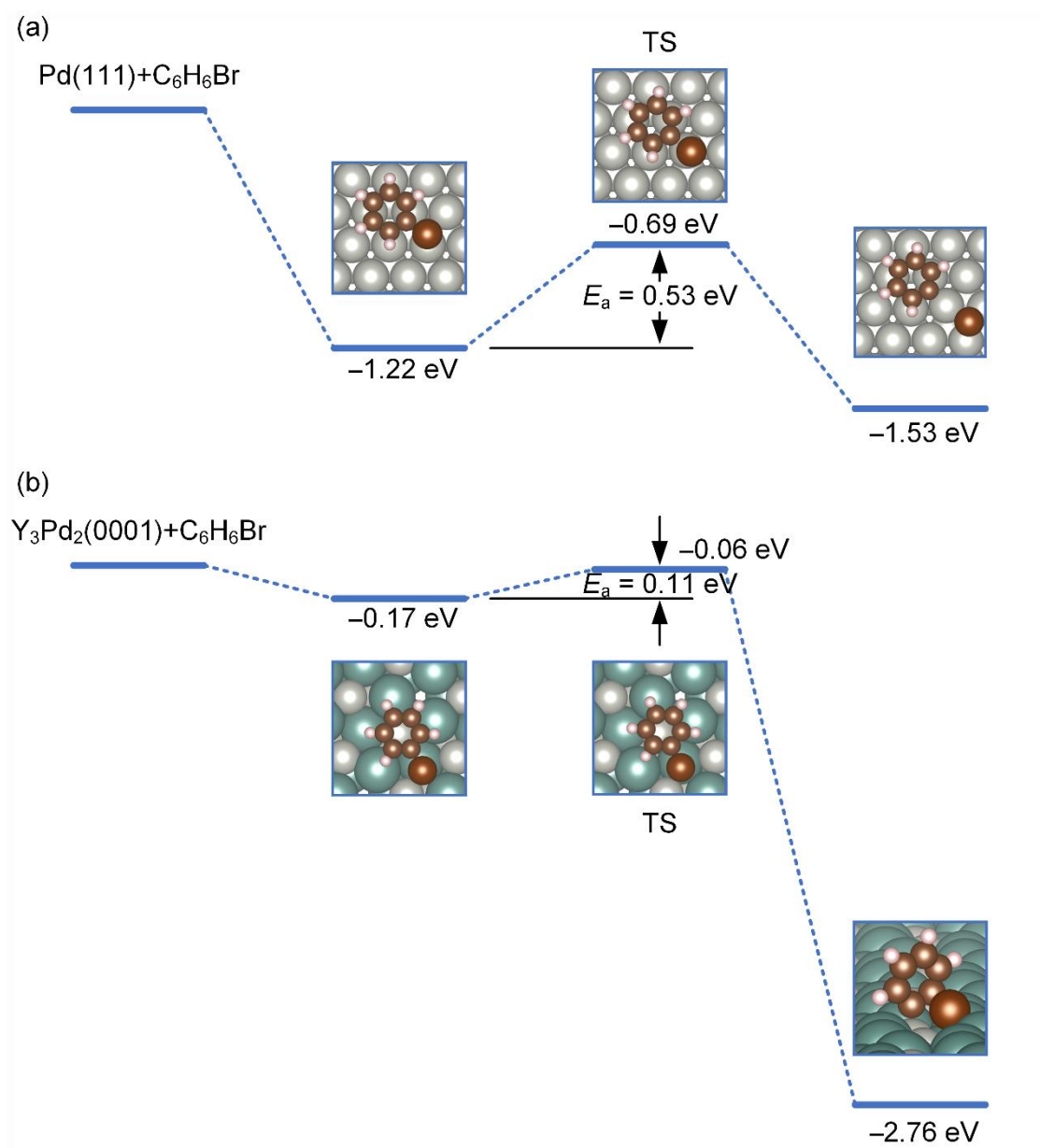
X = Br



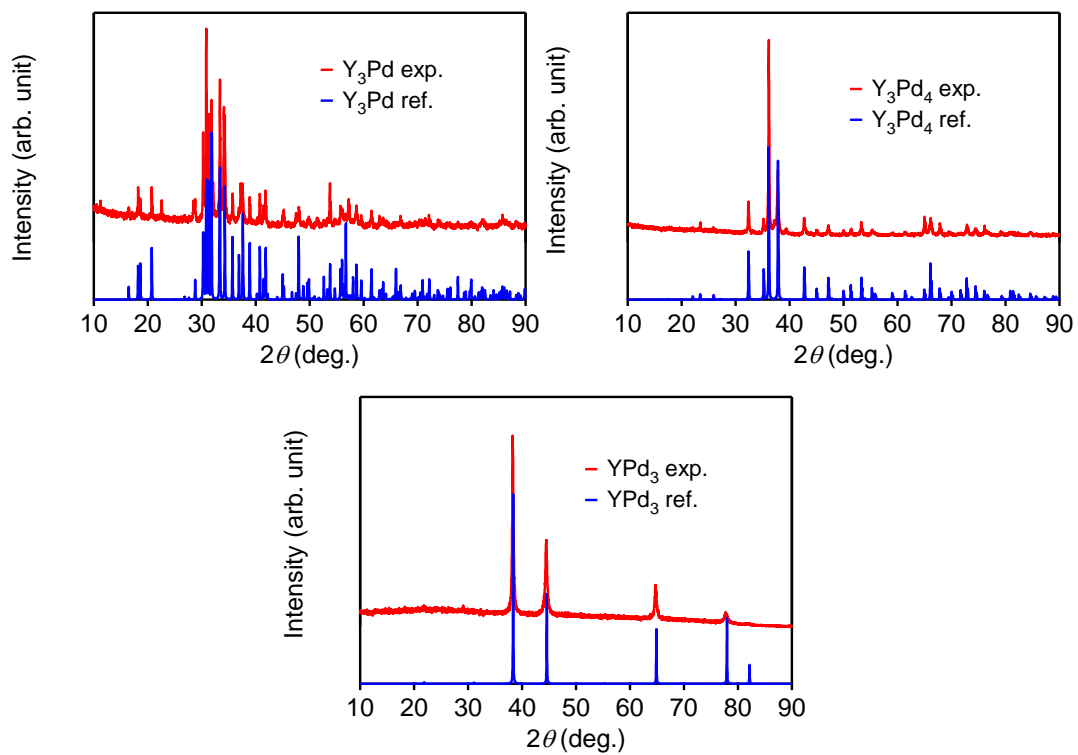
Supplementary Figure 12 a, c. Dependences of reaction rate on aryl halides (iodo and bromo) concentration over the Y_3Pd_2 catalyst. b, d. Dependences of reaction rate on phenylboronic acid concentration over the Y_3Pd_2 catalyst. Reaction conditions: Pd (40 mol% relative to organohalide), 1.5 mmol K_2CO_3 , 5ml solvent, iodides 30 °C, bromides 60 °C.



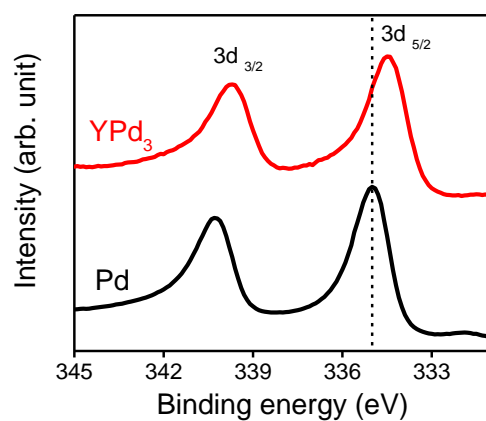
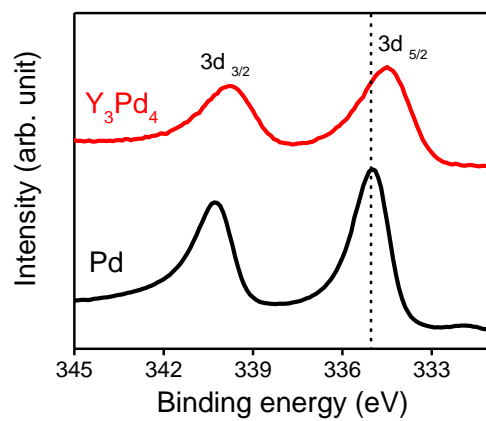
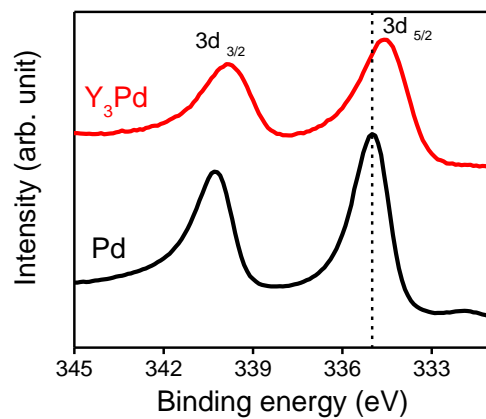
Supplementary Figure 13 Top views of (a) Pd(111) and (b) Y₃Pd₂(0001) surfaces.



Supplementary Figure 14 Energy profiles of C₆H₅Br activation over (a) Pd(111) and (b) Y₃Pd₂(0001) surfaces.

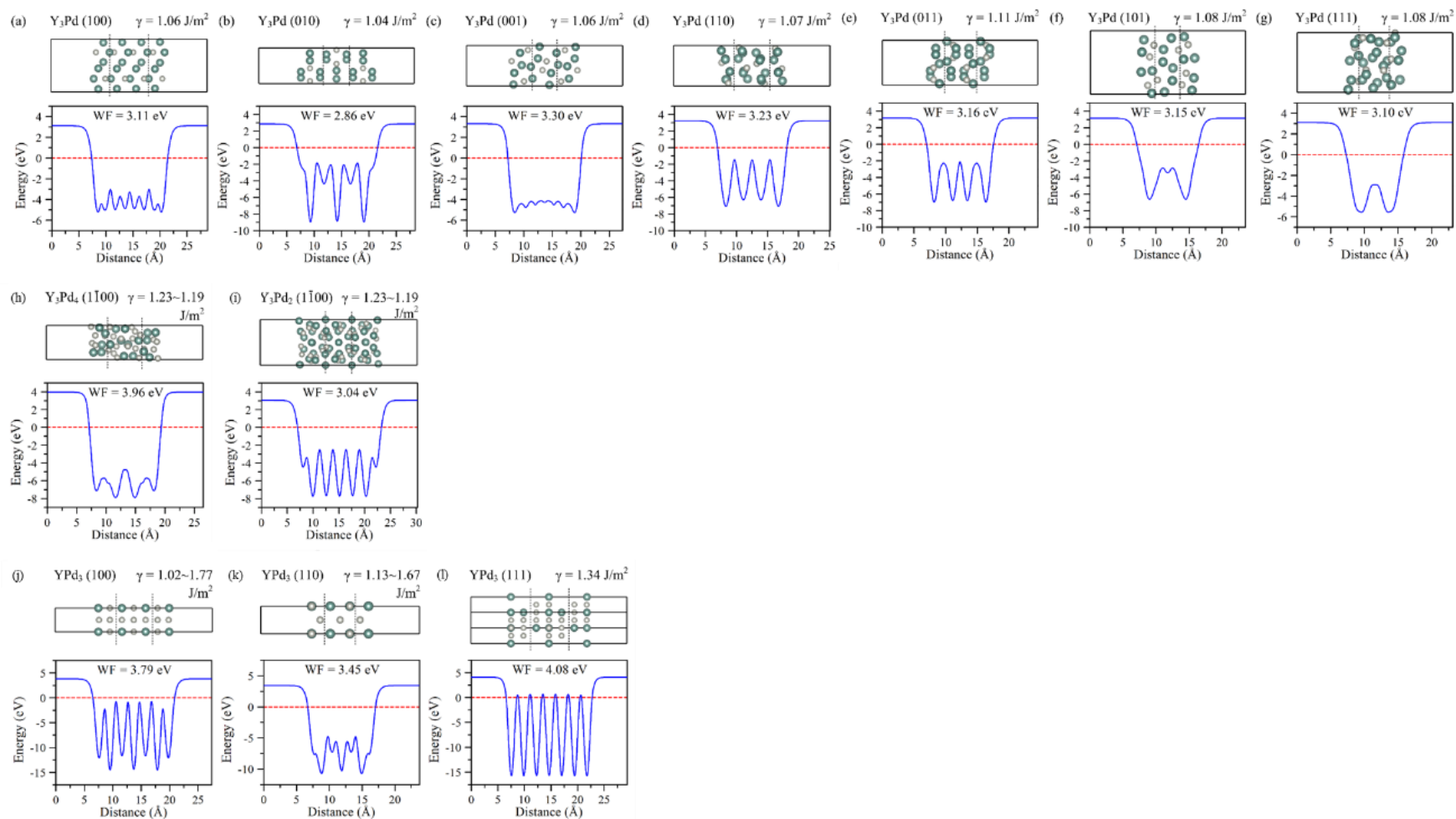


Supplementary Figure 15 | Powder XRD pattern of Y_3Pd , Y_3Pd_4 and YPd_3 . The red and blue solid lines represent experimentally obtained and calculated pattern.

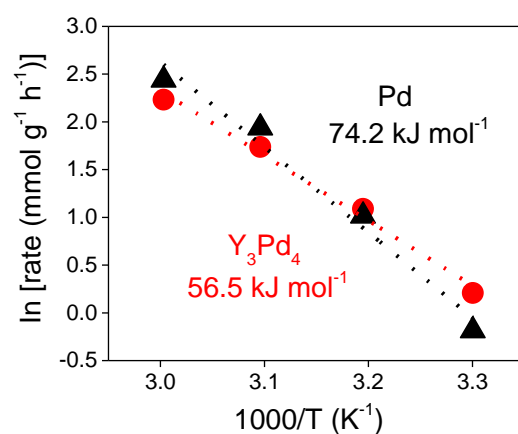
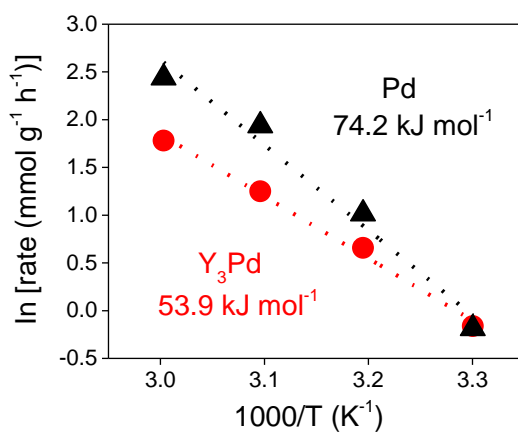
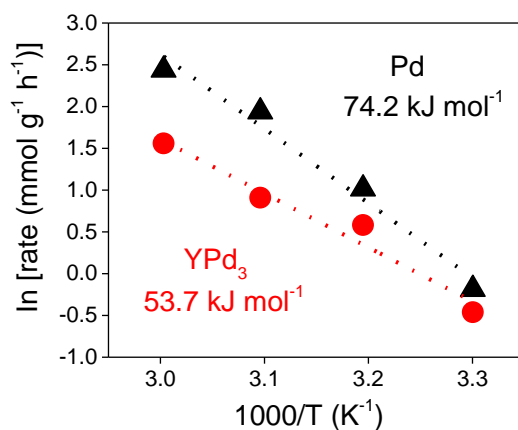


Supplementary Figure 16 | XPS Pd 3d spectra for the Pd, Y₃Pd, Y₃Pd₄ and YPd₃ catalyst.

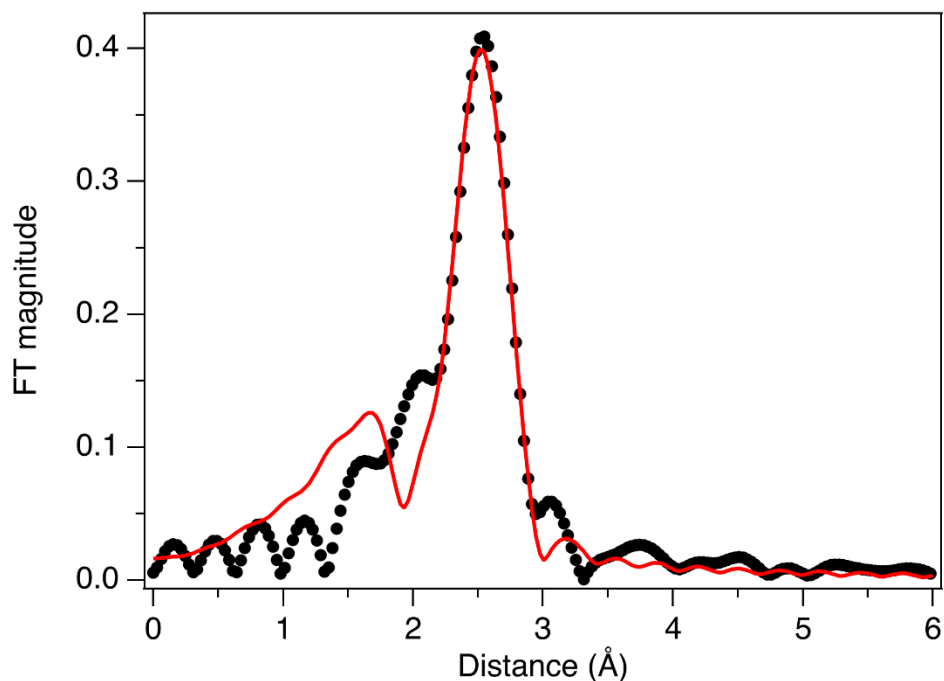
The XPS measurements revealed obvious red shifts of typical Pd 3d peaks, indicating the Pd active sites in these compounds were also negative charged.



Supplementary Figure 17 | Calculated work functions of Y_3Pd , Y_3Pd_4 and YPd_3 . The corresponding slab models and surface energies are also given. The red dashed lines indicate the Fermi levels.



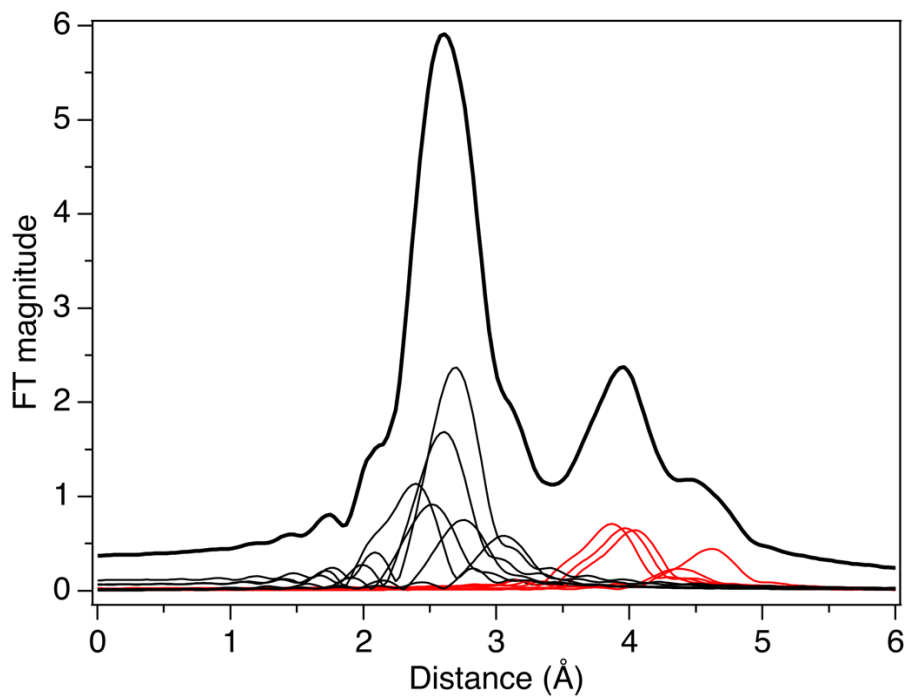
Supplementary Figure 18 | Apparent E_a for the Suzuki coupling reaction over Y_3Pd , Y_3Pd_4 and YPd_3 compounds and pure Pd metal catalysts. Reaction conditions: Pd (40 mol% relative to organohalide); 0.5 mmol iodobenzene, 0.8 mmol phenylboronic acid, 1.5 mmol K_2CO_3 , 5 mL solvent. An error analysis was performed for these data and the error range was determined to be $\pm 5\%$.



Supplementary Figure 19 | EXAFS fitting result by Y_3Pd_2 structure. The R-factor is 0.082.

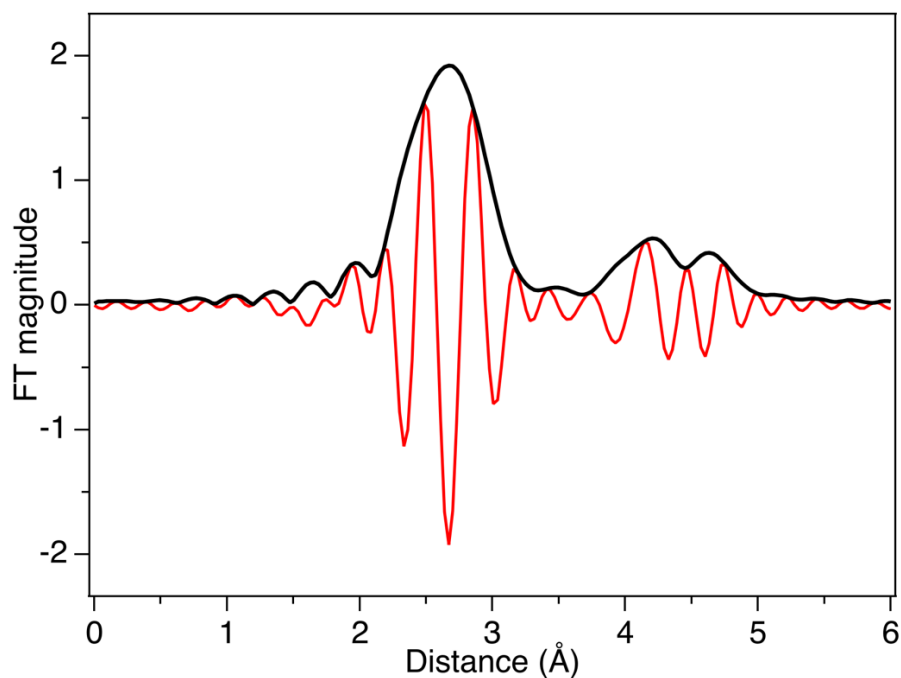
Black dots denote the experimental data, and red line the fitting curve.

Another additional EXAFS fitting in order to check the stoichiometry was also performed. With keeping Y_3Pd_2 geometry, the amplitudes of Pd-Pd and Pd-Y paths in the EXAFS fitting procedure were independently fitted each other. The as-fitted numbers gave $Y_{3.57}Pd_{2.09}$. If the numbers are normalized by Y number to 3, it goes to $Y_3Pd_{1.75}$. Considering fitting errors, this estimated composition is in a good agreement with the bulk 3:2 stoichiometry.

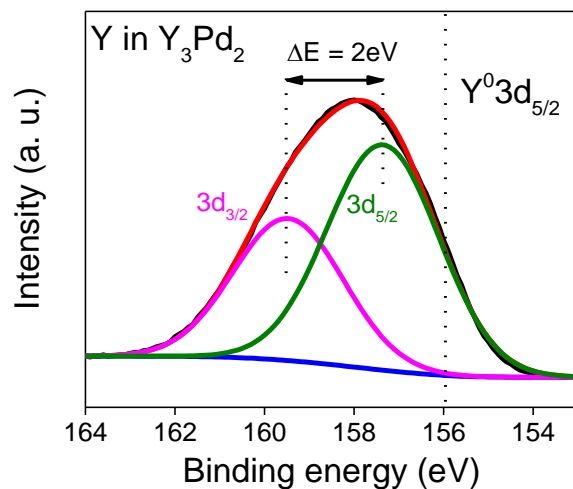


Supplementary Figure 20 | FEFF simulated amplitudes of paths for the ideal Y_3Pd_2 structure.

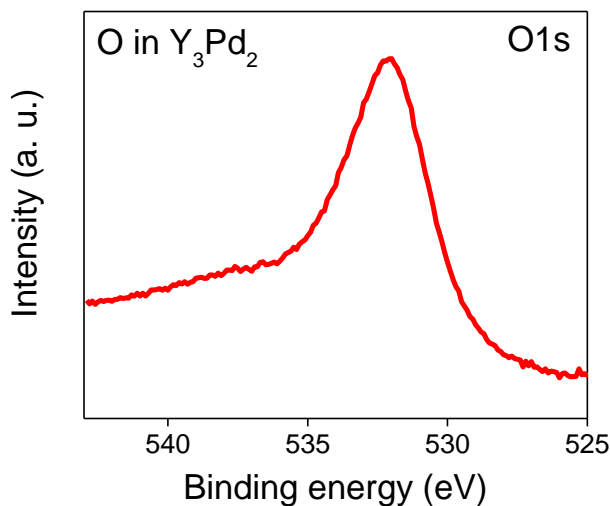
Thin lines denote the amplitudes of the paths, and the red ones represent long range paths. All the amplitudes of the paths summed up to black bold line. Note that this black bold line does not correspond to the real EXAFS FT, because the phases of the paths should be considered. See text and Supplementary Figure 21.



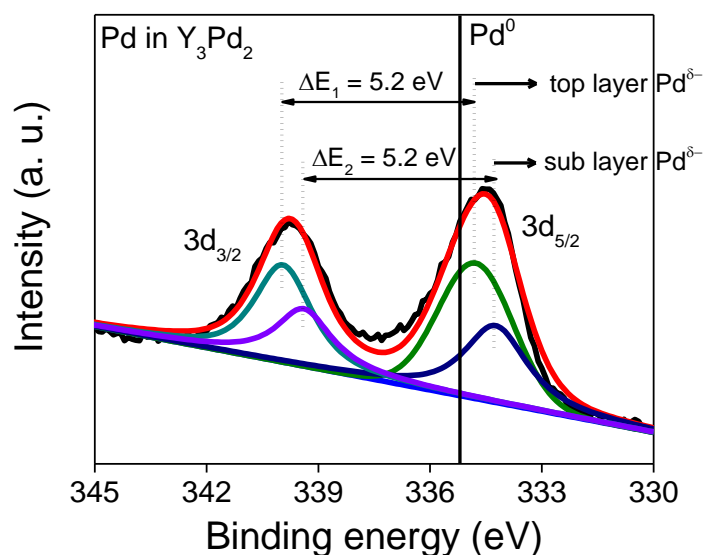
Supplementary Figure 21 The sum of the imaginary parts of the paths simulated for the ideal Y_3Pd_2 structure (red line) and its envelop function (black bold line). A few peaks are still found around 4 Å, but the intensities are not strong compared to Supplementary Figure 20. Note that this is the simulation based on the ideal Y_3Pd_2 structure and that the real structure is more or less deviated. The deviations in addition to thermal vibrations and some other effects like multiple scattering weaken long range peaks. Consequently, strong peaks in the long range were not observed in EXAFS FT (Supplementary Figure 19).



Supplementary Figure 22 | XPS analysis of Y 3d spectra in Y_3Pd_2 . Here, Y 3d peaks gave a significantly shift to higher energy compared to that of $Y^0 3d$, indicating that Y is positively charged in Y_3Pd_2 .



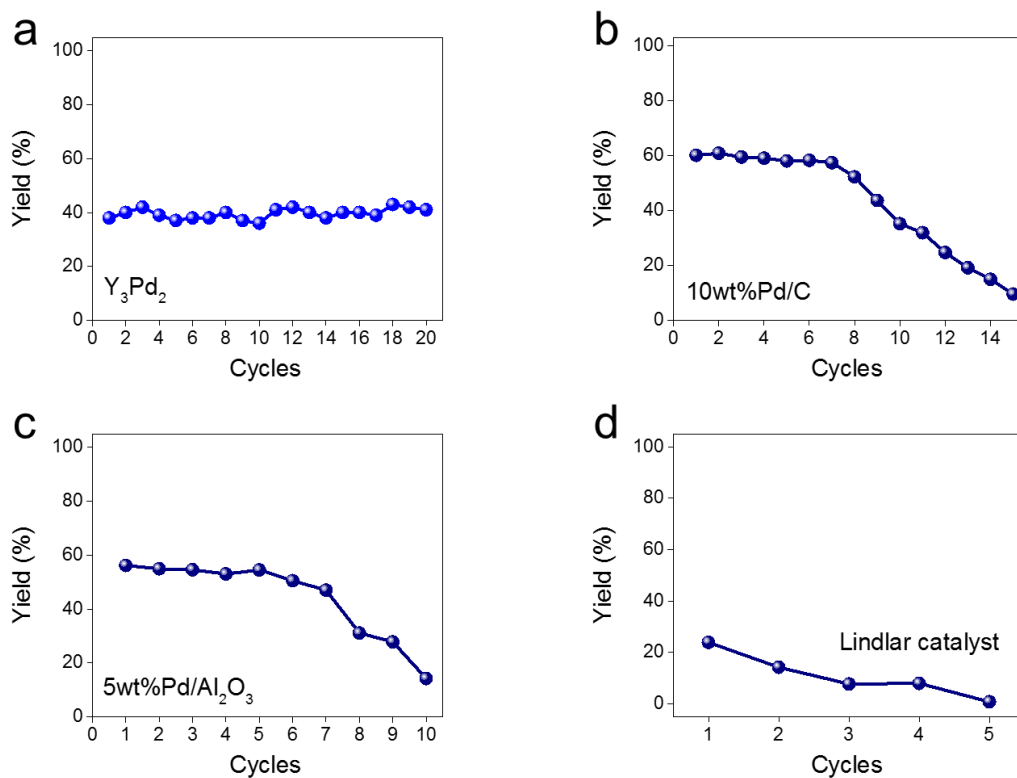
Supplementary Figure 23 | XPS analysis of O 1s spectra in Y_3Pd_2 . It is reported that the binding energy at 529.1 eV was originated from the Y-O bond in stoichiometric Y_2O_3 film.¹ Here, O 1s spectra in Y_3Pd_2 gave no obvious peak at 529.1 eV compared to that of Y_2O_3 , indicating that the generation of surface Y-oxide can also be ruled out.



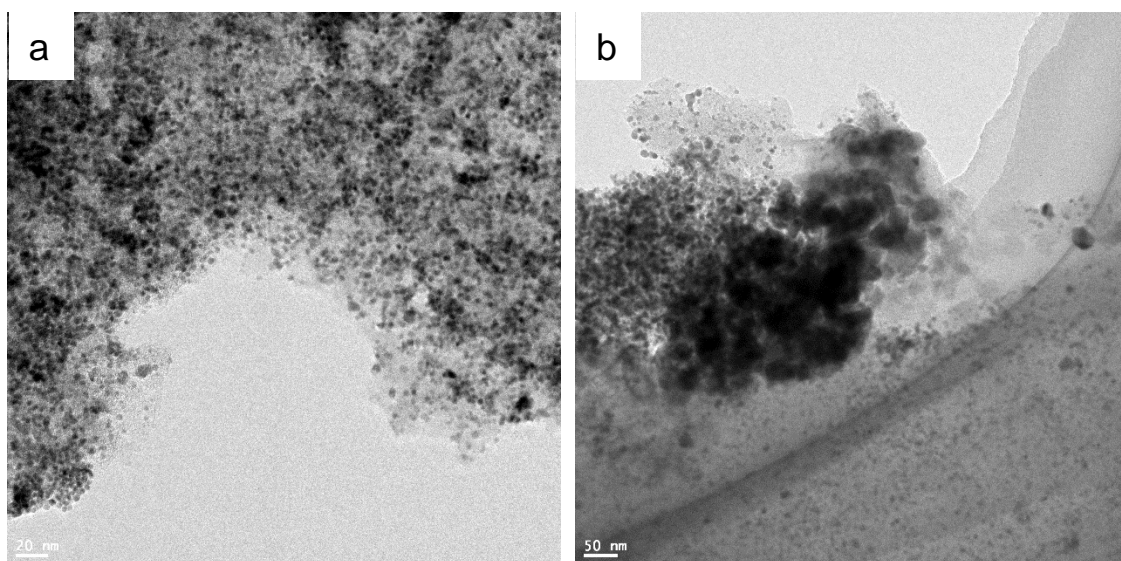
Supplementary Figure 24 | XPS analysis of Pd 3d spectra in Y_3Pd_2 . Here, Pd 3d peaks gave a significantly shift to lower energy compared to that of Pd^0 3d, indicating that Pd is negative charged in Y_3Pd_2 .

Normally, the binding energy peak position of a specific element depends on the oxidation state and local chemical environment. In the case of modifying a sample by adding other elements, if the electronegativity of the doped element (like Y in our case) is lower than the base element (like Pd in our case), the electron density around the base element (like Pd in our case) increases and the binding energy decreases. Therefore, the binding energy peak of Pd shifts negatively compared with the zero valence state Pd metal.

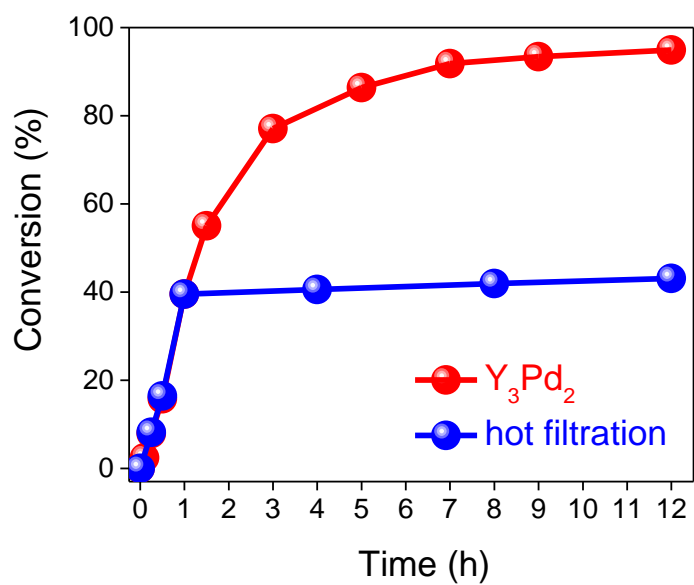
In Y_3Pd_2 , for the top layer, Pd coordinated by lower coordination dominates the surface, which gave a negative charged Pd state with a negatively shifted binding energy. For the bulk, fully coordinated Pd species constituted the sub layer and deeper layers, resulting in a much negatively charged state with a more negatively shifted binding energy compared to the top layer Pd. This is because of the existence of more coordinated Y electron donors that can increase the electron density of those bulk Pd species. Both kinds of electronic structure of Pd states appeared in the XPS spectra with the detection limit of several atomic layer thickness of Y_3Pd_2 surface, which is in good agreement with our Bader charge analysis.



Supplementary Figure 25 Recycling experiment for the Suzuki cross-coupling reaction over a. Y_3Pd_2 ; b. 10wt%Pd/C; c. 5wt%Pd/ Al_2O_3 ; d. 5wt%Pd Lindlar catalyst. Reaction conditions: Y_3Pd_2 , Pd (40 mol% relative to organohalide); 10wt%Pd/C (20 mg); 5wt%Pd/ Al_2O_3 (20 mg); 5wt%Pd Lindlar catalyst (20 mg); 0.5 mmol iodobenzene, 0.8 mmol phenylboronic acid, 1.5 mmol K_2CO_3 , 5mL solvent, 30 °C, 1 h. An error analysis was performed for these data and the error range was determined to be $\pm 5\%$.

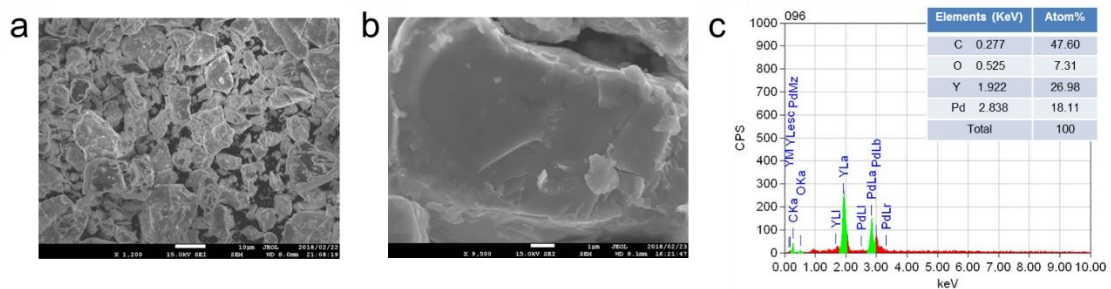


Supplementary Figure 26 TEM images of the commercial 10wt%Pd/C catalyst used as a reference **a.** before and **b.** after 15 cyclic reactions. Reaction conditions: 10wt%Pd/C (20 mg), 0.5 mmol iodobenzene, 0.8 mmol phenylboronic acid, 1.5 mmol K_2CO_3 , 5mL solvent, 30 °C, 1h. Clear aggregation of Pd can be confirmed for the used catalyst.

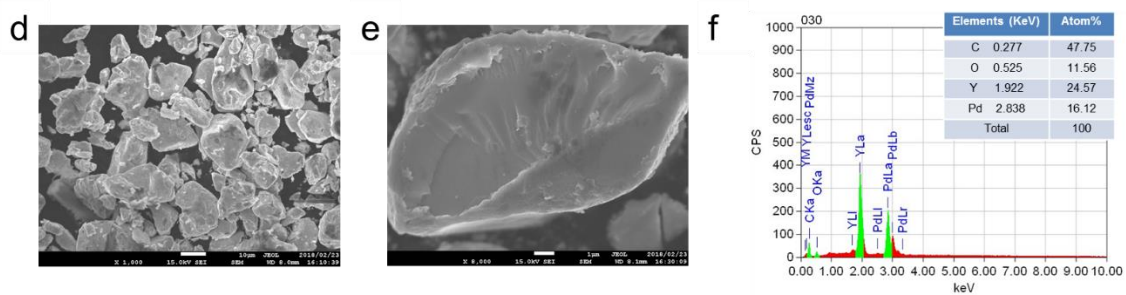


Supplementary Figure 27 | Hot filtration test of Y_3Pd_2 for Suzuki coupling reaction. The reaction no longer proceeds after removal of the Y_3Pd_2 catalyst. Reaction conditions: Pd (40 mol% relative to organohalide); 0.5 mmol iodides, 0.8 mmol phenylboronic acid, 1.5 mmol K_2CO_3 , 5ml solvent, 30 °C.

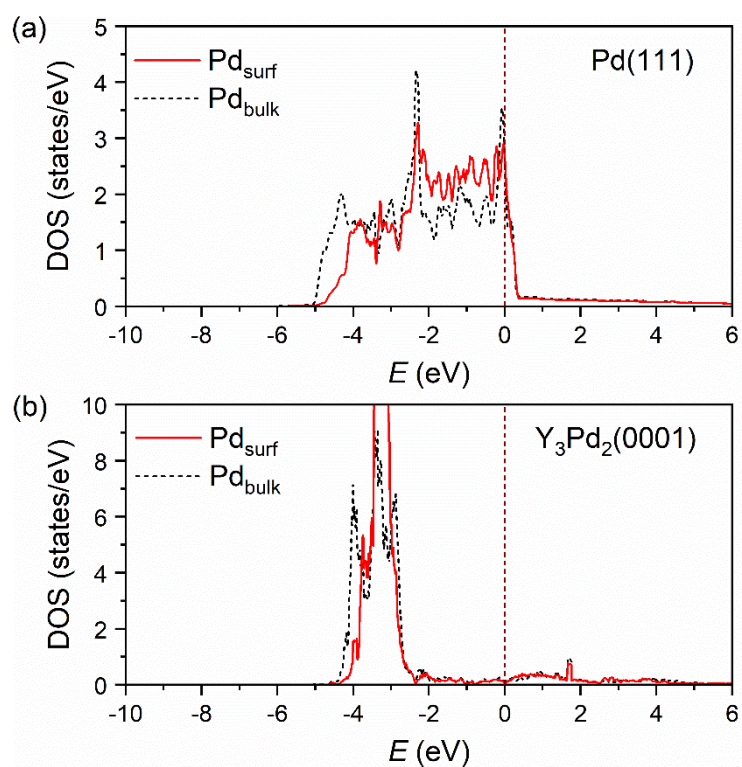
Before



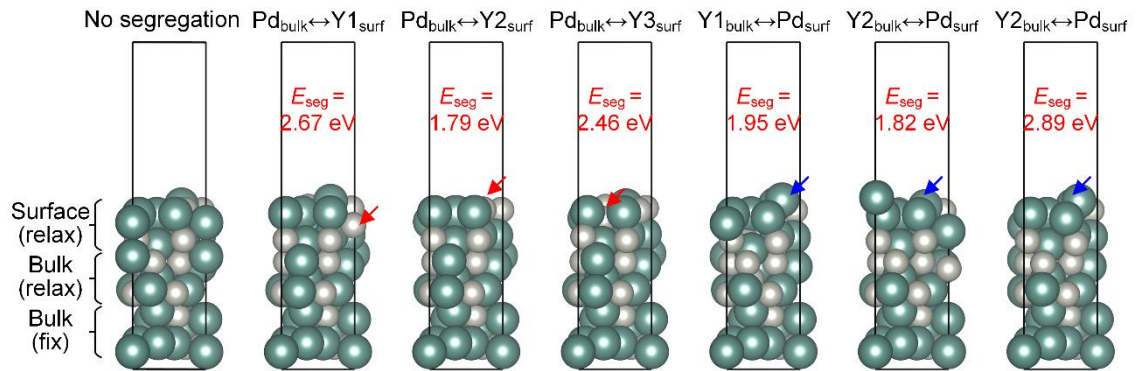
After



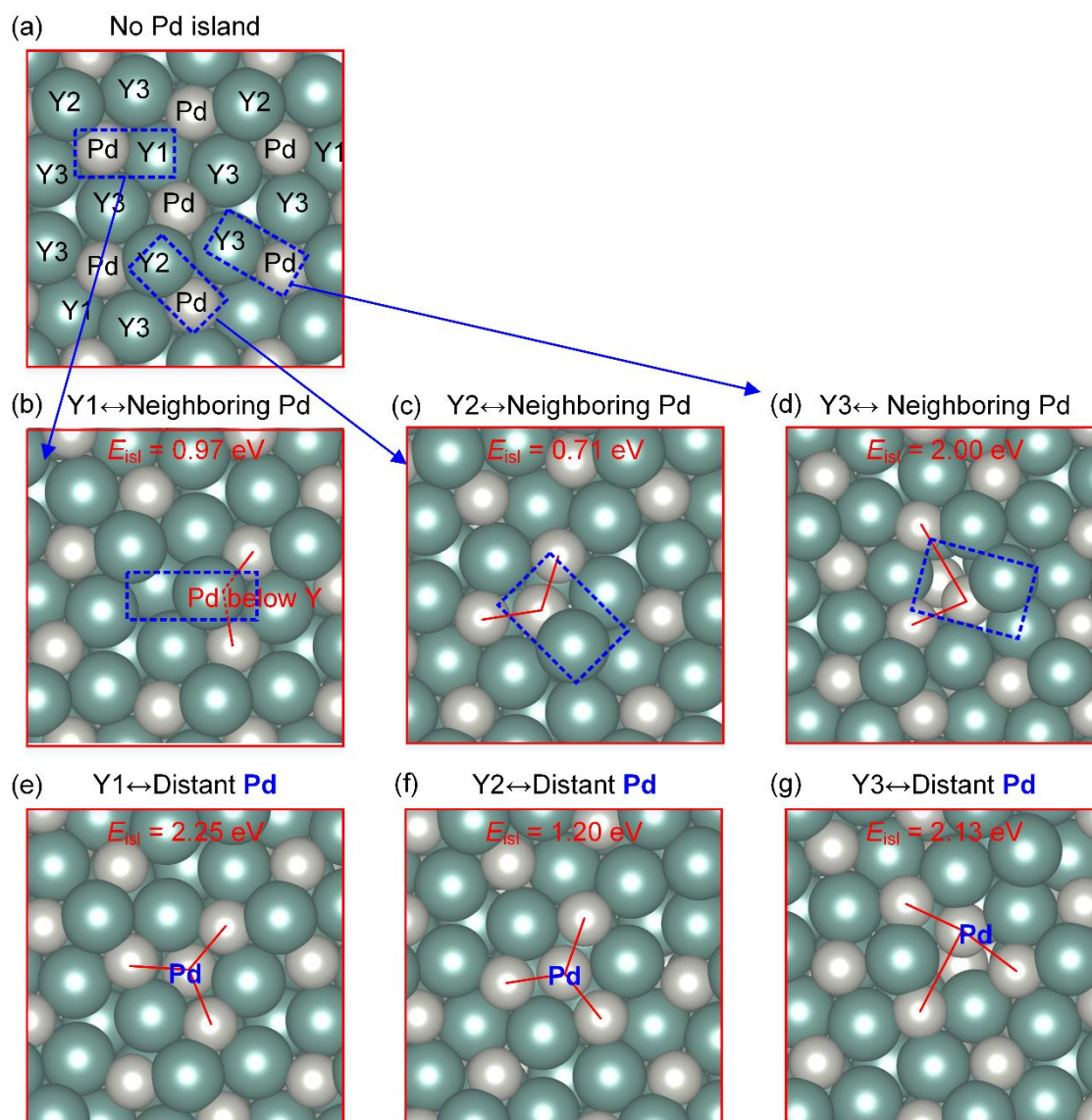
Supplementary Figure 28 SEM images and EDS spectra of the as-prepared and used Y_3Pd_2 catalyst.



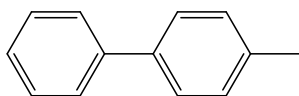
Supplementary Figure 29 Projected Pd *d*-band densities of states (DOS). The *d*-band center (ϵ_d) is at -0.95 , -1.23 , -2.31 , and -2.30 eV for the Pd atoms on the surface and in the bulk of Pd(111) and Y₃Pd₂(0001), respectively.



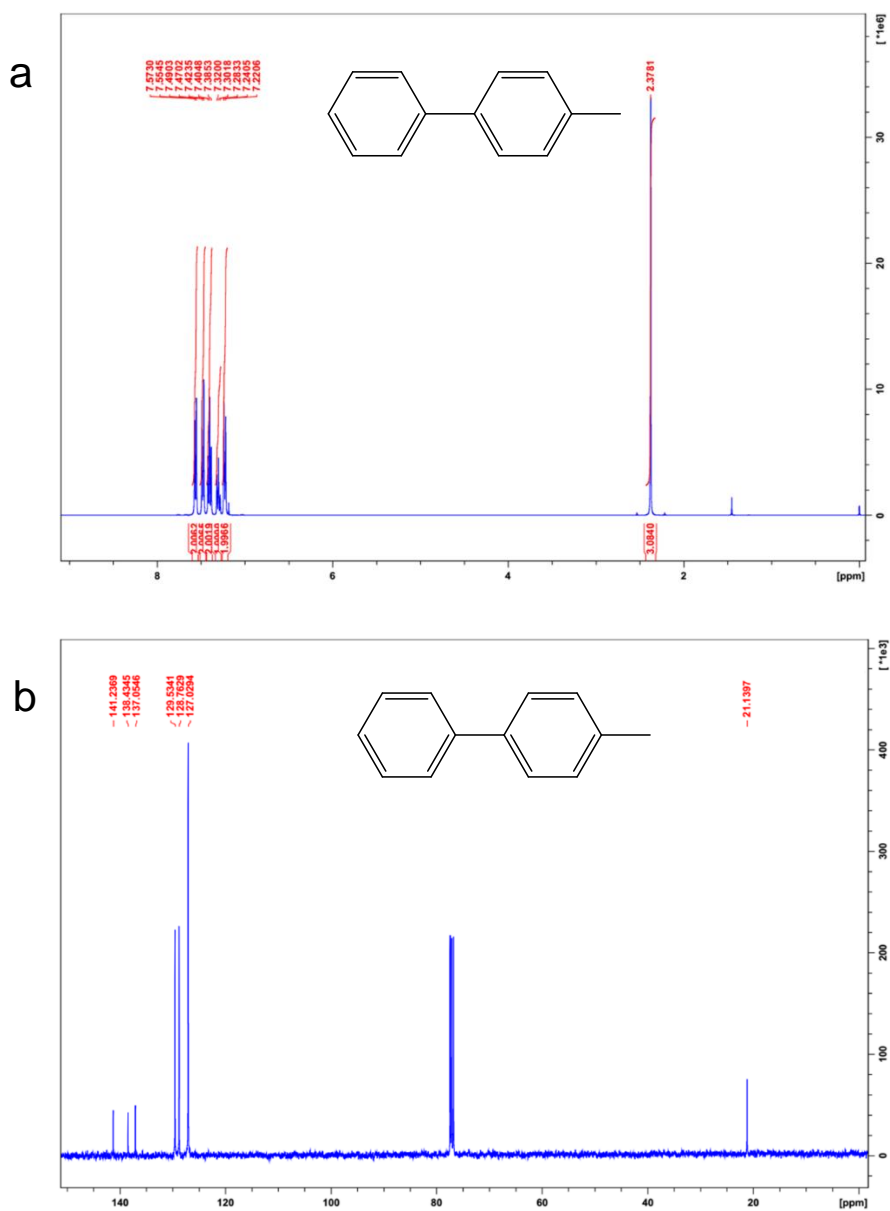
Supplementary Figure 30 Side view of the relaxed $\text{Y}_3\text{Pd}_2(0001)$ surface structures without and with Pd and Y segregations. The Pd atoms marked with red arrow are the ones segregated from the bulk to the different Y atoms sites on the surface. The Y atoms marked with blue arrow are the ones segregated from the bulk to the Pd site on the surface. The segregation energies (E_{seg}) of Pd and Y atoms are 1.79–2.67 and 1.82–2.89 eV, respectively.



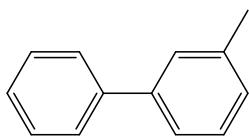
Supplementary Figure 31 Top view of the relaxed surface structures without and with Pd islands: (a) No island; (b–c) Islands formed by replacing Y1, Y2, Y3 with a neighboring Pd atom; (e–f) Islands formed by replacing Y1, Y2, Y3 atoms with a distant Pd atom. The island formation energies (E_{isl}) of Pd range from 0.71 to 2.25 eV.



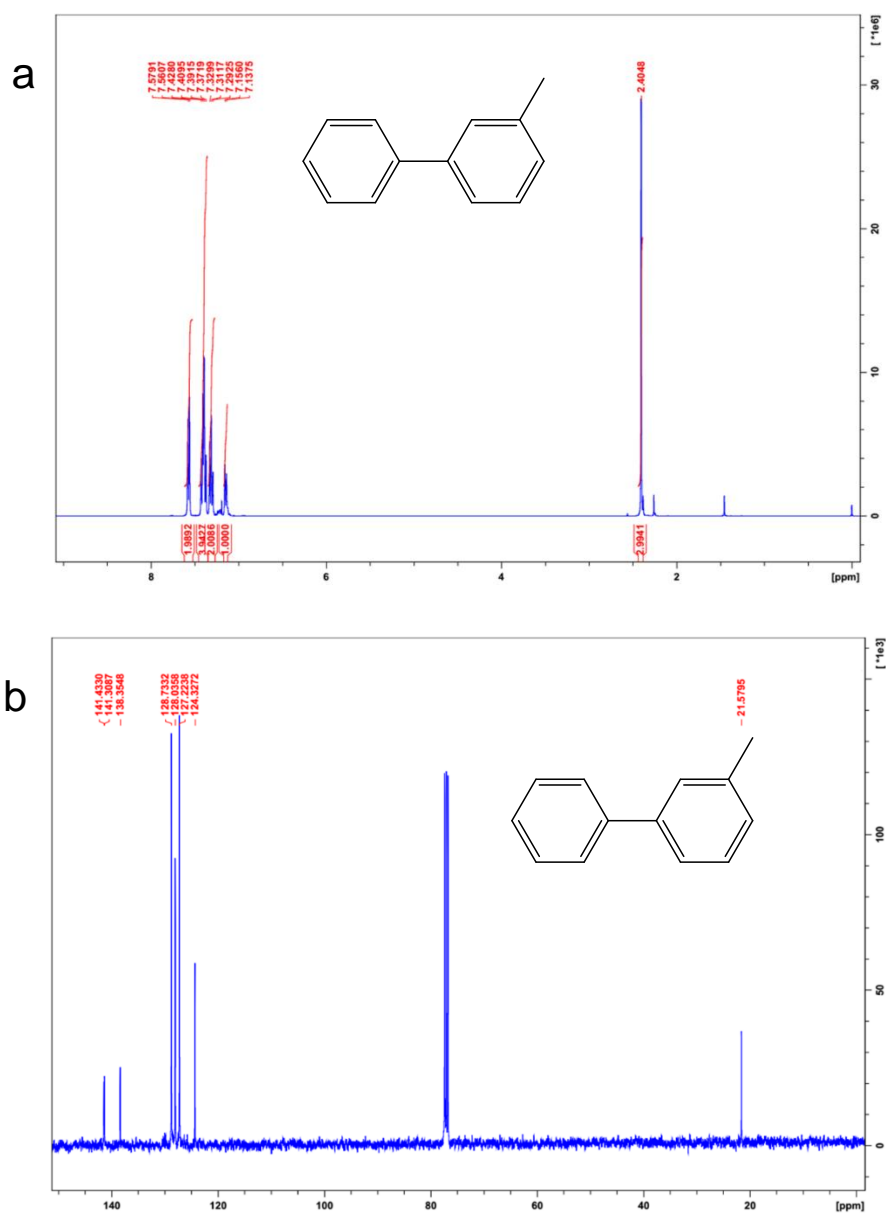
^1H NMR (CDCl_3 , 400 MHz): $\delta = 7.56$ (d, 2H), 7.48 (d, 2H), 7.40 (t, 2H), 7.30 (t, 1H), 7.23 (d, 2H), 2.38 (s, 3H); ^{13}C NMR (CDCl_3 , 100 MHz): $\delta = 141.2$, 138.4, 137.1, 129.5, 128.8, 127.0, 21.1.



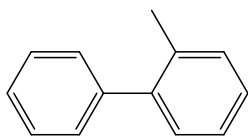
Supplementary Figure 32 a. ^1H NMR and b. ^{13}C NMR spectra.



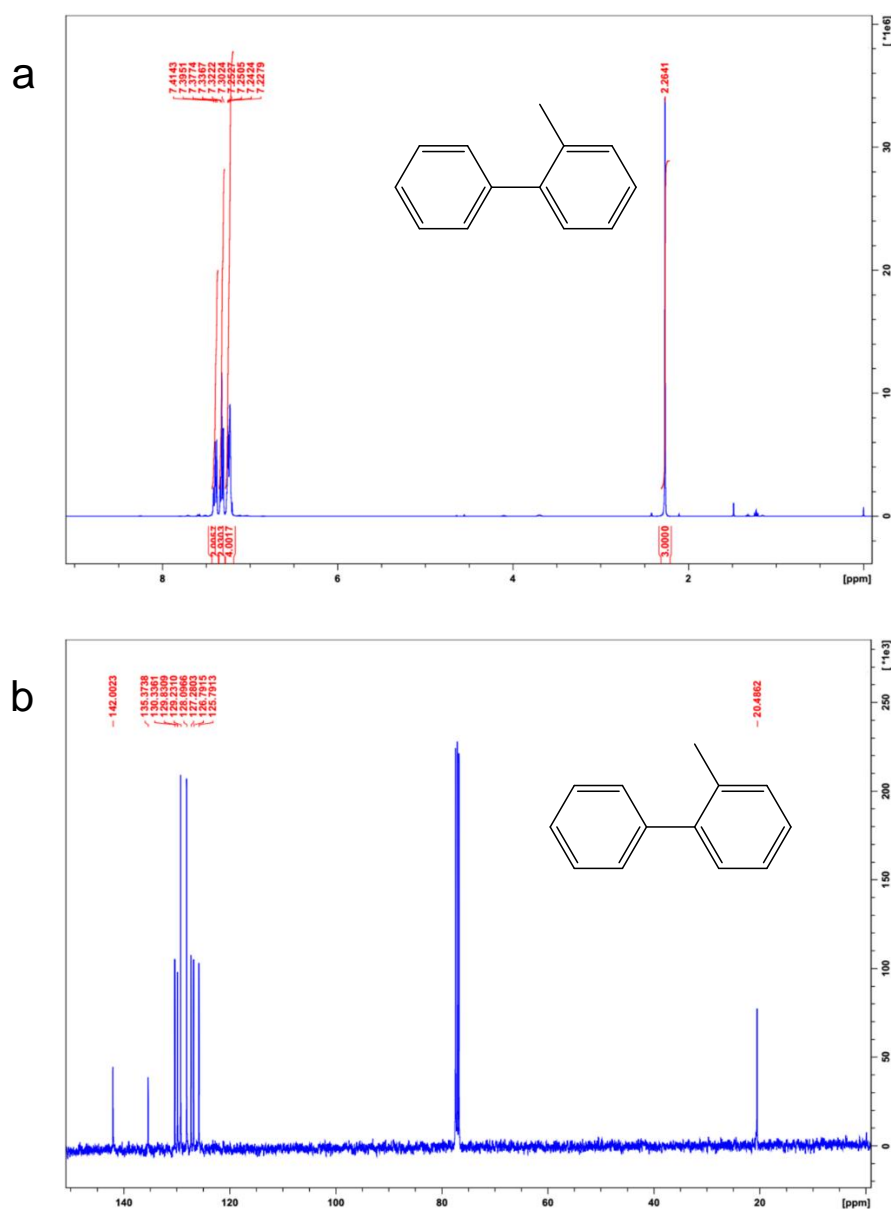
^1H NMR (CDCl_3 , 400 MHz): $\delta = 7.57$ (d, 2H), 7.45-7.35 (m, 4H), 7.31 (t, 2H), 7.15 (d, 1H), 2.40 (s, 3H); ^{13}C NMR (CDCl_3 , 100 MHz): $\delta = 141.4$, 141.3, 138.4, 128.7, 128.0, 127.2, 124.3, 21.6.



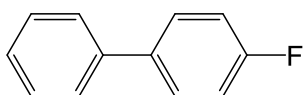
Supplementary Figure 33 a. ^1H NMR and b. ^{13}C NMR spectra.



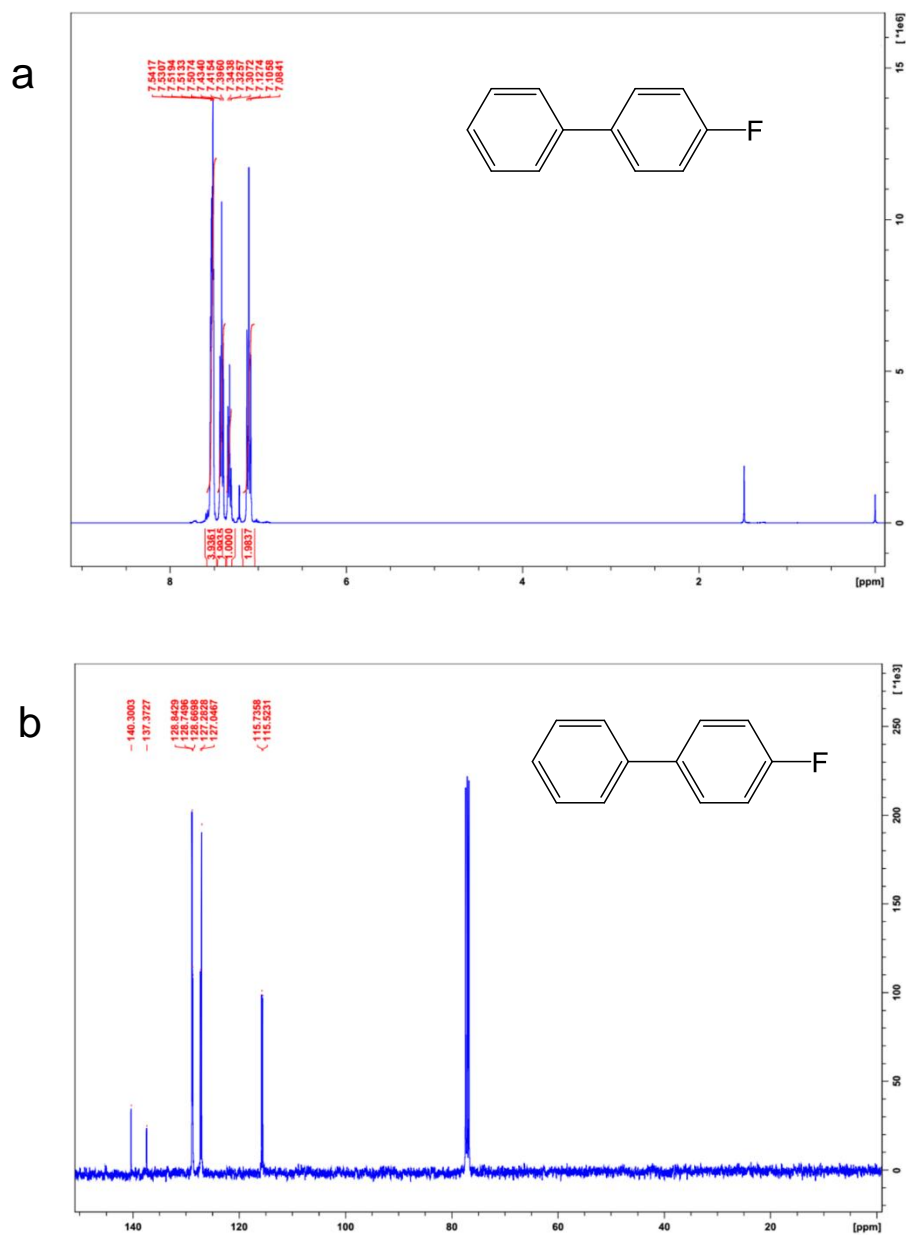
^1H NMR (CDCl_3 , 400 MHz): $\delta = 7.40$ (t, 2H), 7.38-7.29 (m, 3H), 7.27-7.21 (m, 4H), 2.26 (s, 3H); ^{13}C NMR (CDCl_3 , 100 MHz): $\delta = 142.0$, 135.4, 130.3, 129.8, 129.2, 128.1, 127.3, 126.8, 125.8, 20.5.

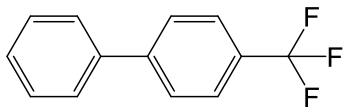


Supplementary Figure 34 a. ^1H NMR and b. ^{13}C NMR spectra.

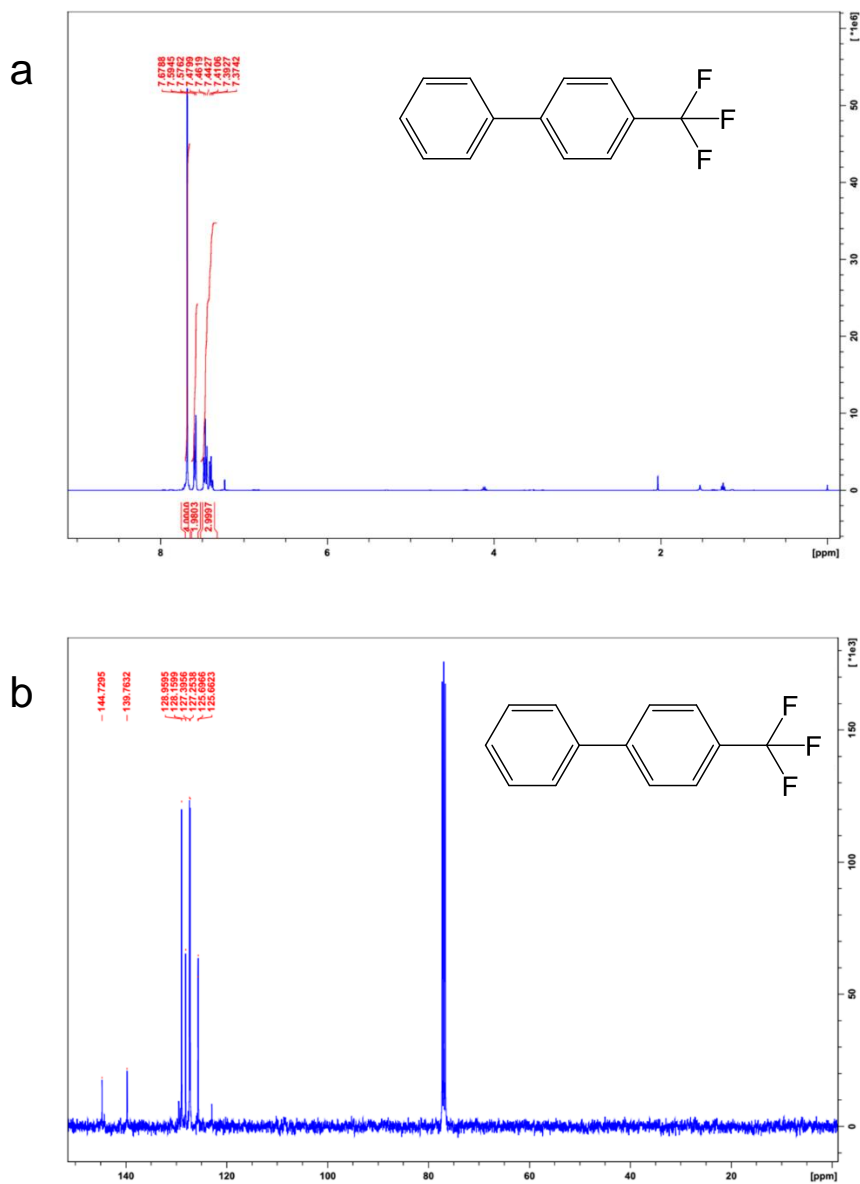


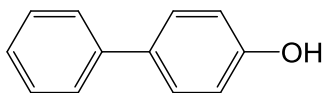
^1H NMR (CDCl_3 , 400 MHz): $\delta = 7.56\text{--}7.48$ (m, 4H), 7.42 (t, 2H), 7.32 (t, 1H), 7.11 (t, 2H); ^{13}C NMR (CDCl_3 , 100 MHz): $\delta = 140.3, 137.4, 128.8, 128.7, 128.6, 127.3, 127.0, 115.7, 115.5$.



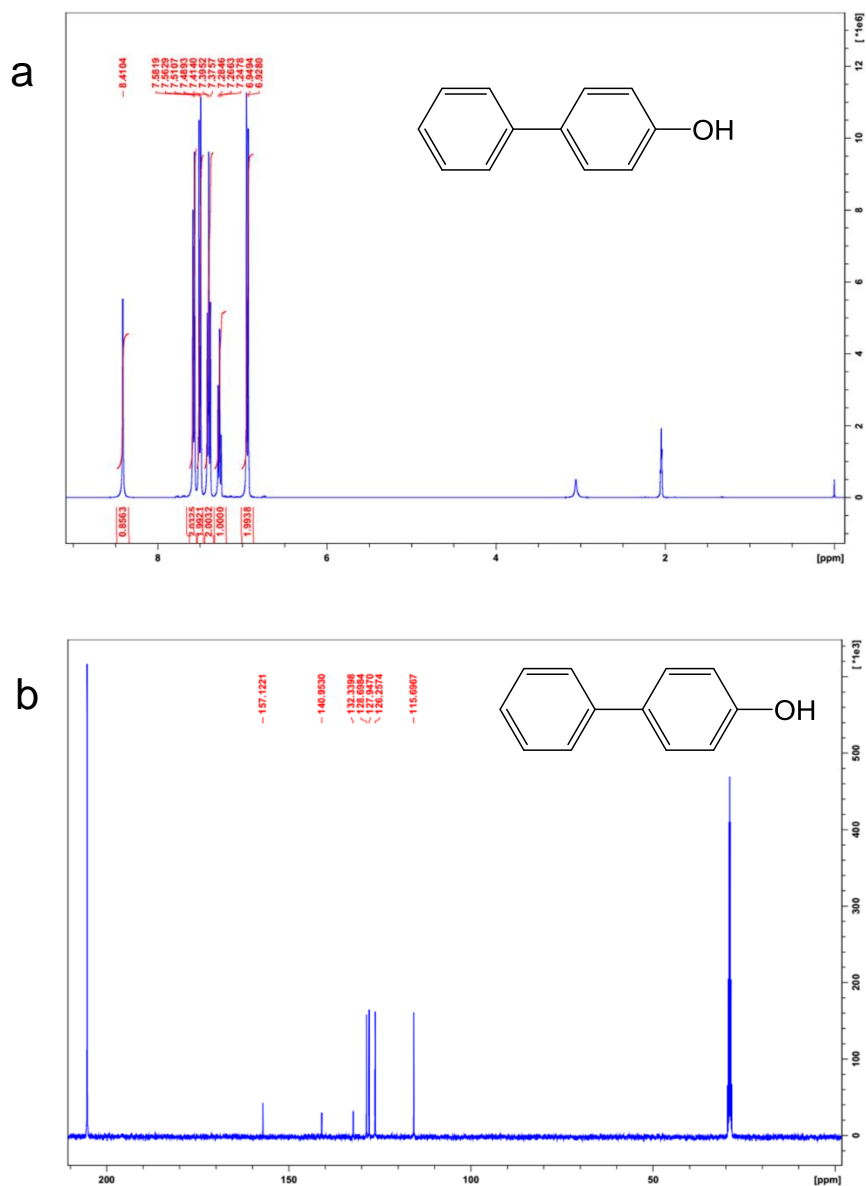


^1H NMR (CDCl_3 , 400 MHz): $\delta = 7.68$ (s, 4H), 7.58 (d, 2H), 7.49-7.35 (m, 3H); ^{13}C NMR (CDCl_3 , 100 MHz): $\delta = 144.7, 139.7, 129.0, 128.2, 127.4, 127.3, 125.7, 125.6$.

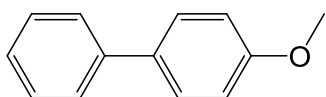




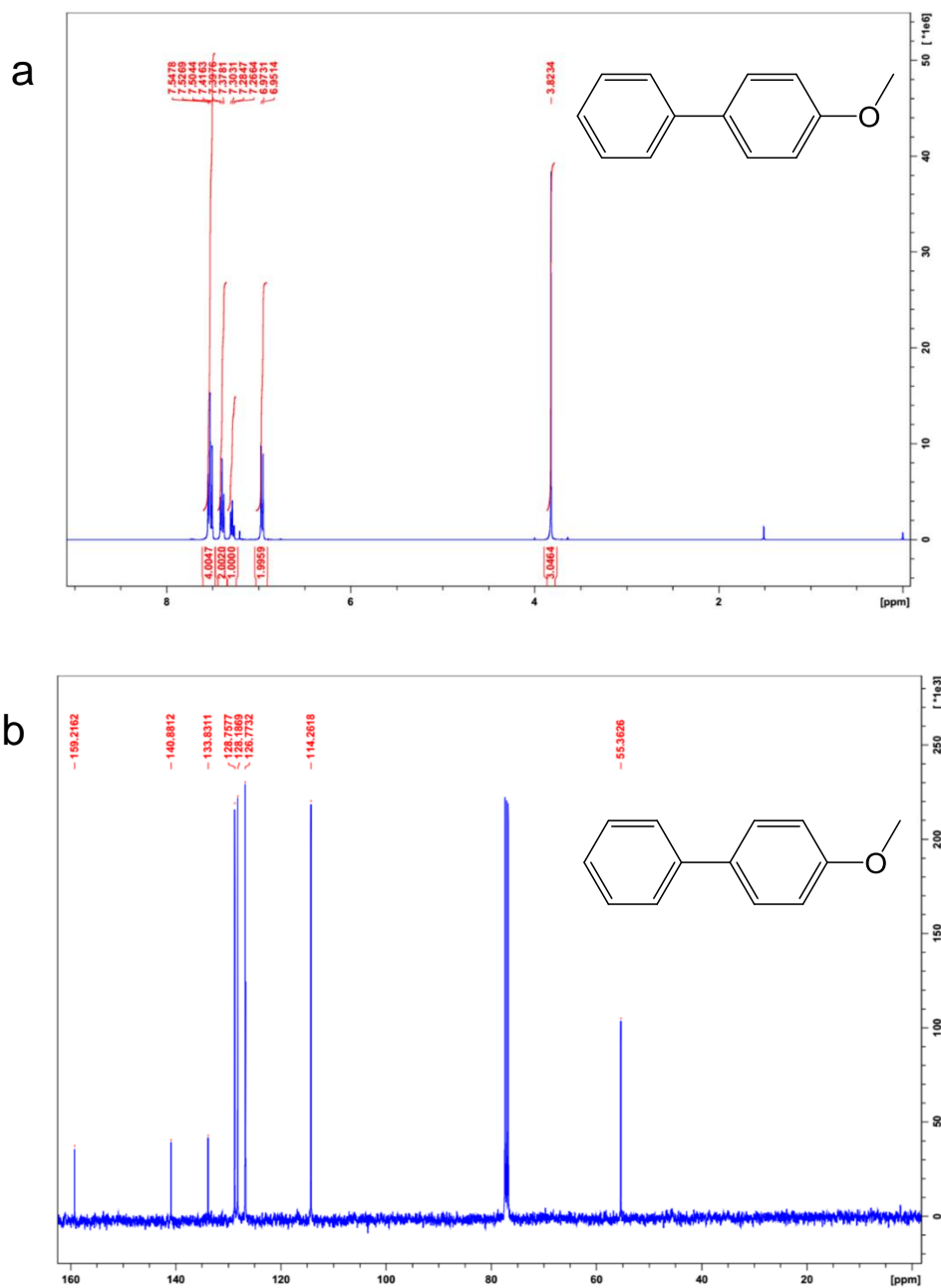
^1H NMR $[(\text{CD}_3)_2\text{CO}, 400 \text{ MHz}]$: $\delta = 8.41$ (s, 1H), 7.57 (d, 2H), 7.50 (d, 2H), 7.40 (t, 2H), 7.27 (t, 1H), 6.94 (d, 2H); ^{13}C NMR $[(\text{CD}_3)_2\text{CO}, 100 \text{ MHz}]$: $\delta = 157.1, 141.0, 132.3, 128.7, 127.9, 126.3, 115.7$.



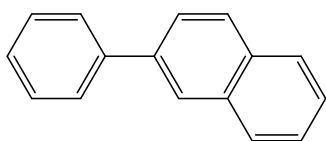
Supplementary Figure 37 a. ^1H NMR and b. ^{13}C NMR spectra.



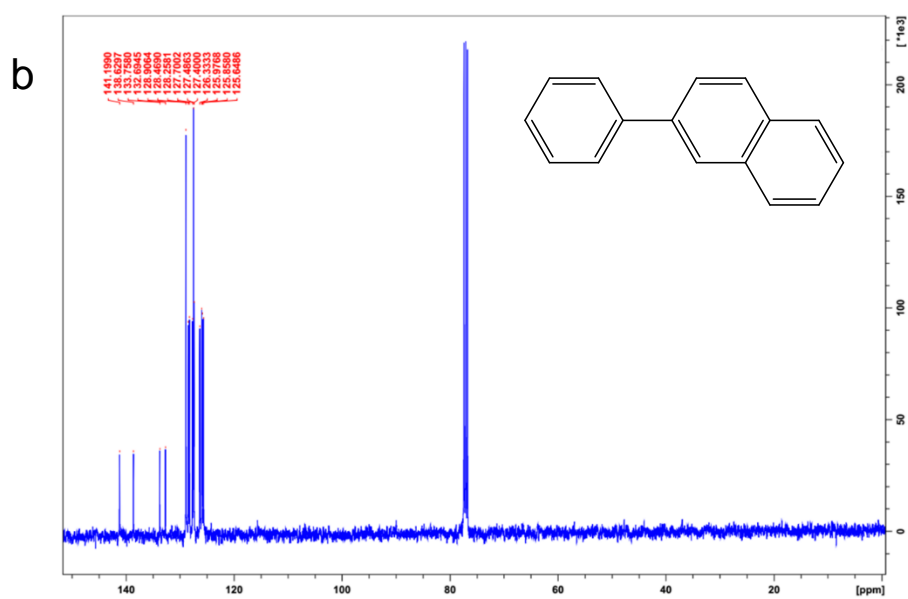
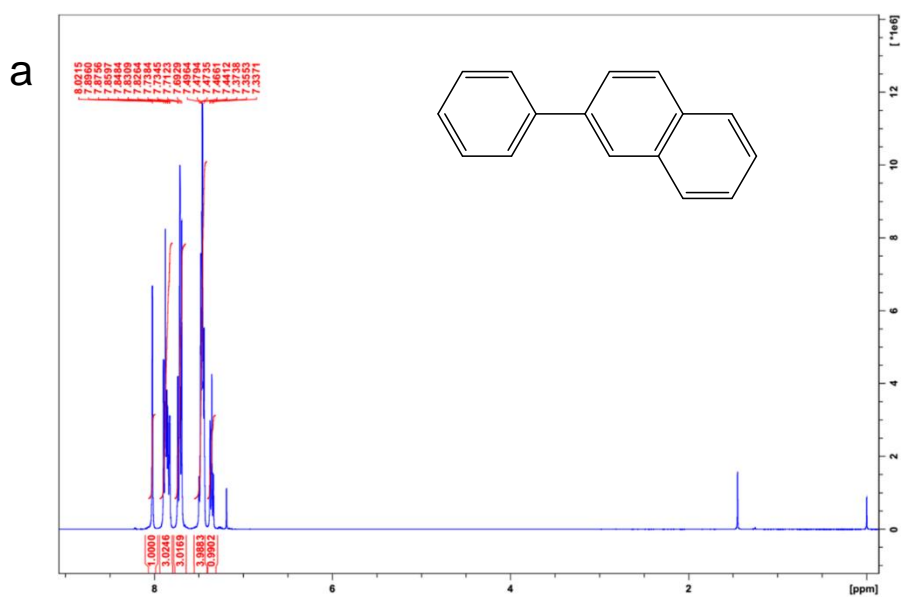
^1H NMR (CDCl_3 , 400 MHz): $\delta = 7.53$ (t, 4H), 7.40 (t, 2H), 7.28 (t, 1H), 6.96 (d, 2H), 3.82 (s, 3H); ^{13}C NMR (CDCl_3 , 100 MHz): $\delta = 159.2$, 140.9, 133.8, 128.8, 128.2, 126.8, 114.3, 55.4.



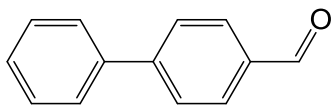
Supplementary Figure 38 a. ^1H NMR and b. ^{13}C NMR spectra.



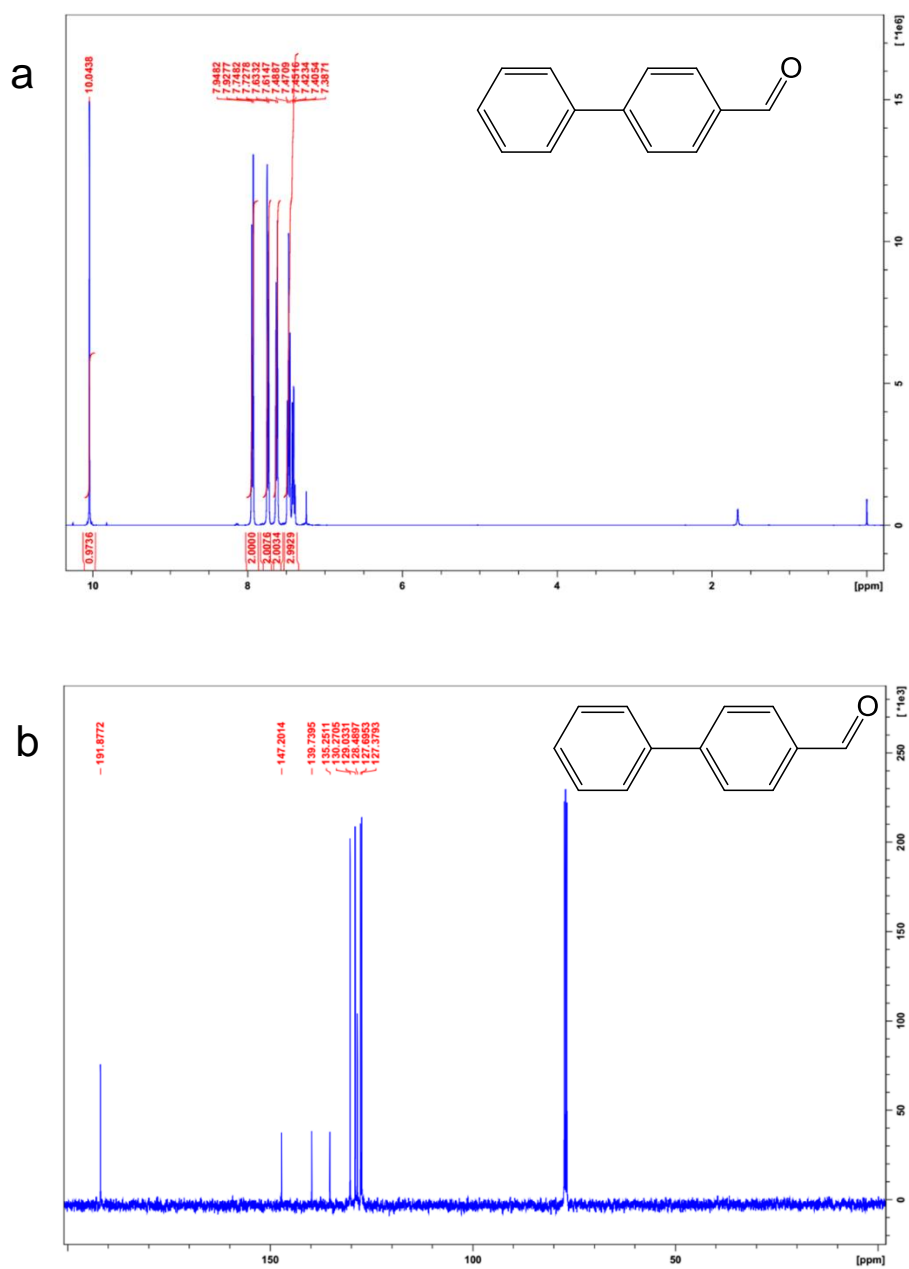
^1H NMR (CDCl_3 , 400 MHz): $\delta = 8.02$ (s, 1H), 7.91-7.83 (m, 3H), 7.83-7.69 (m, 3H), 7.50-7.37 (m, 4H), 7.38-7.33 (m, 1H); ^{13}C NMR (CDCl_3 , 100 MHz): $\delta = 141.2$, 138.6, 133.8, 132.7, 128.9, 128.5, 128.3, 127.7, 127.5, 127.4, 126.3, 126.0, 125.9, 125.6.

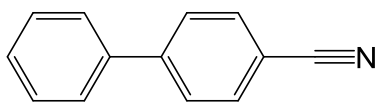


Supplementary Figure 39 a. ^1H NMR and b. ^{13}C NMR spectra.

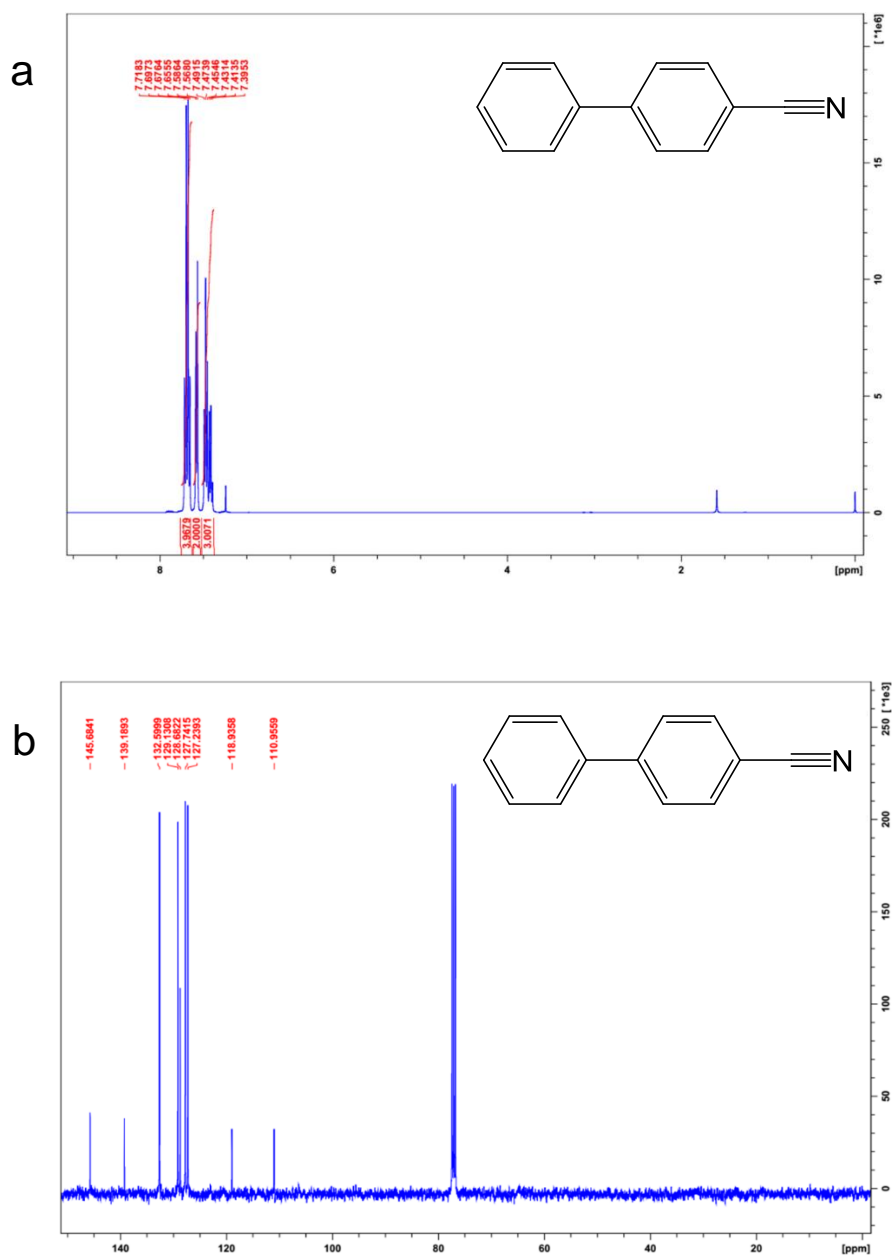


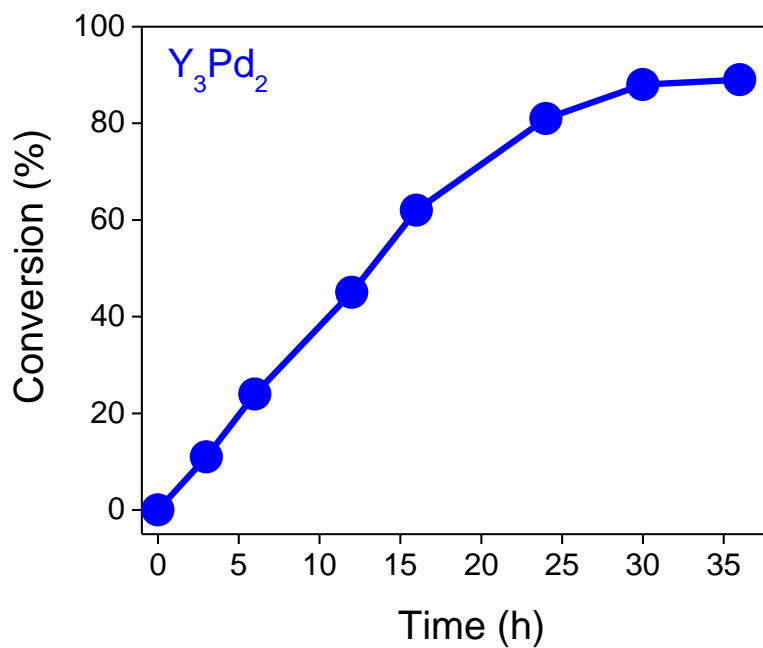
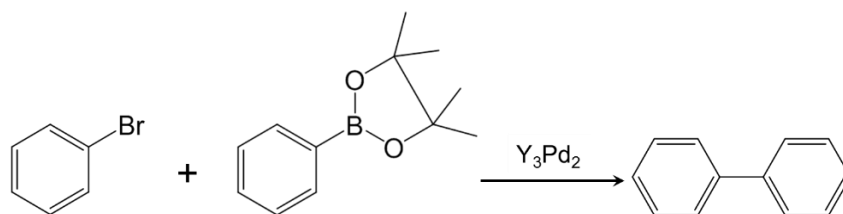
^1H NMR (CDCl_3 , 400 MHz): δ = 10.0 (s, 1H), 7.94 (d, 2H), 7.74 (d, 2H), 7.62 (d, 2H), 7.49-7.38 (m, 3H); ^{13}C NMR (CDCl_3 , 100 MHz): δ = 191.9, 147.2, 139.7, 135.3, 130.3, 129.0, 128.5, 127.7, 127.4.





^1H NMR (CDCl_3 , 400 MHz): $\delta = 7.72\text{--}7.65$ (m, 4H), 7.59–7.56 (d, 2H), 7.50–7.39 (m, 3H);
 ^{13}C NMR (CDCl_3 , 75 MHz): $\delta = 145.7, 139.2, 132.6, 129.1, 128.7, 127.7, 127.2, 118.9, 111.0$.





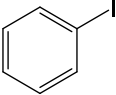
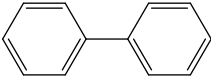
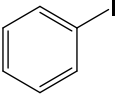
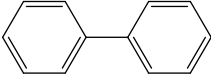
Supplementary Figure 42 Time-dependent catalysis over Y_3Pd_2 catalyst for Suzuki coupling reaction of bromobenzene with phenyl boronic acid pinacol ester. Reaction conditions: Pd (40 mol% relative to organohalide); 0.5 mmol bromobenzene, 0.8 mmol phenylboronic acid pinacol ester, 1.5 mmol K_2CO_3 , 5 mL solvent, 60 °C. An error analysis was performed for these data and the error range was determined to be $\pm 5\%$.

Supplementary Table 1 Catalytic performance of Y₃Pd₂ and Pd

| Sample | iodobenzene | | | bromobenzene | | |
|--------------------------------|--|---|----------------|---|---|----------------|
| | TOFs based on surface Pd by unit cell (h ⁻¹) | TOFs based on total Pd (h ⁻¹) | Carbon balance | TOFs based on surface Pd by unit cell Pd (h ⁻¹) | TOFs based on total Pd (h ⁻¹) | Carbon balance |
| Y ₃ Pd ₂ | 1670.1 | 7.6 | 98.1% | 4034.4 | 7.33 | 99.1% |
| Pd | 129.3 | 0.9 | 98.4% | 355 | 2.25 | 98.9% |

Reaction conditions: Pd (40 mol% relative to organohalide); 0.5 mmol organohalide, 0.8 mmol phenylboronic acid, 1.5 mmol K₂CO₃, 5mL solvent, iodides 30 °C, bromides 60 °C. Carbon balance was calculated by the consumption of the substrate iodobenzene and the yield of the biphenyl, respectively, through the analysis of GC and GC-MS. An error analysis was performed for these data and the error range was determined to be ±5%.

Supplementary Table 2 Ullmann coupling reactions of iodobenzene with iodobenzene over Y_3Pd_2 and pure Pd.

| Entry | Catalyst | Substrate | Product | Time (h) | Yield (%) |
|-------|-----------|---|--|----------|-----------|
| 1 | Y_3Pd_2 |  |  | 24 | trace |
| 2 | Pd |  |  | 24 | trace |

Reaction conditions: Pd (40 mol% relative to organohalide); 0.5 mmol iodobenzene, 1.5 mmol K_2CO_3 , 5 mL solvent, 30 °C. An error analysis was performed for these data and the error range was determined to be $\pm 5\%$.

Supplementary Table 3 Catalytic performance comparison of Y₃Pd₂ with commercial heterogeneous Pd-based catalysts.

| Catalyst | Surface area (m ² g ⁻¹) | CO _{ads} . (ml g ⁻¹) | Exposed Pd by CO _{ads} . (10 ⁻⁶ mol g ⁻¹) | Reaction rate (mmol g ⁻¹ h ⁻¹) | TOFs (h ⁻¹) |
|--|---|--|---|--|----------------------------|
| ^a Y ₃ Pd ₂ | 0.431 | 0.0198 | 0.9 | 3.04 | 3378 |
| ^b Y ₃ Pd ₂ | 3.2 | 0.1312 | 5.9 | 17.02 | 2934 |
| ^c Pd/C | 526.5 | 0.8810 | 78.6 | 15.2 | 193 |
| ^d Pd/Al ₂ O ₃ | 96.8 | 1.991 | 177.8 | 14.1 | 79 |
| ^e Pd-Pb/CaCO ₃ | 6.9 | 0.1496 | 13.4 | 5.98 | 446 |

Reaction conditions: ^aPd (40 mol% relative to organohalide); ^bY₃Pd₂ ball-milled by ethanol, Pd (40 mol% relative to organohalide); ^c10wt%Pd/C (20 mg); ^d5wt%Pd/Al₂O₃ (20 mg); ^e5wt%Pd Lindlar catalyst (20 mg); 0.5 mmol iodobenzene, 0.8 mmol phenylboronic acid, 1.5 mmol K₂CO₃, 5mL solvent, 30 °C. A stoichiometry of Pd/CO = 1 was used for Y₃Pd₂ and Pd/CO = 2 for Pd/C, Pd/Al₂O₃ and Lindlar catalyst. An error analysis was performed for these data and the error range was determined to be ±5%.

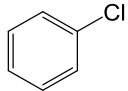
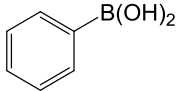
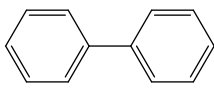
Supplementary Table 4 Summary of results reported for different Pd-based catalysts in the coupling of iodobenzene and phenylboronic acid

| Catalyst | Condition | TOF (h ⁻¹) | Recycle No | Reference |
|-------------------------------------|---|------------------------|------------|------------------|
| Y₃Pd₂ | EtOH, K₂CO₃ 30 °C, 1 h | 1670.1 | 20 | This work |
| Pd/MFC | EtOH, K ₂ CO ₃ Reflux, 1 h | 324.6 | 5 | 2 |
| Pd NPs | H ₂ O, Na ₂ CO ₃ 80 °C, 24h | 40.5 | 6 | 3 |
| Pd/Fe ₃ O ₄ | DME-H ₂ O, Na ₂ CO ₃ Reflux, 24h | 41.3 | 10 | 4 |
| Pd@Mag-MSN | CH ₂ Cl ₂ , K ₂ CO ₃ 80 °C, 6h | 14.2 | 3 | 5 |
| Pd/CNT-SiC | EtOH-H ₂ O, K ₃ PO ₄ 80 °C, 1h | 350 | 6 | 6 |
| Pd@CNPCs | DMF-H ₂ O, K ₂ CO ₃ 50 °C, 1.5h | 644.6 | 5 | 7 |
| MUA-Pd | DMF, NaOH 90 °C, 8h | 6.2 | 5 | 8 |
| Pd-CNT-ED-OH | DMF, Na ₂ CO ₃ 110 °C, 24h | 13.1 | 7 | 9 |
| Pd(0)/MCoS-1 | H ₂ O, K ₂ CO ₃ 70 °C, 5h | 98 | 6 | 10 |
| Pd/NiFe ₂ O ₄ | DMF-H ₂ O, Na ₂ CO ₃ 90 °C, 5mins | 196 | 4 | 11 |
| Sugar-derived PdNPs | iPrOH, KCO ₃ 100 °C, 20h | 4.4 | 4 | 12 |
| G/MWCNTs/Pd | EtOH-H ₂ O, K ₂ CO ₃ 60 °C, 15mins | 799 | 6 | 13 |

Supplementary Table 5 Comparison of the activity of Y₃Pd₂ with other results reported Pd-based heterogeneous photocatalyzed Suzuki reactions under visible light

| Catalyst | Condition | TOF (h ⁻¹) | Recycle No | Reference |
|------------------------------------|--|---------------------------------|------------|------------------|
| Y₃Pd₂ | EtOH, K₂CO₃ 30 °C, 1 h | 1670.1 (iodobenzene) | 20 | This work |
| Pd/SiC | DMF-H ₂ O, Cs ₂ CO ₃ 30 °C, 80mins | 1053 (iodobenzene) | 5 | 14 |
| m-CNR-Pd | EtOH-H ₂ O, K ₂ CO ₃ RT, 1h | 51.6 (iodobenzene) | 6 | 15 |
| Pd/Au/PN-CeO ₂ | DMF-H ₂ O, K ₂ CO ₃ 30 °C, 30mins | 6.3 (iodobenzene) | 6 | 16 |
| Y₃Pd₂ | EtOH, K₂CO₃ 60 °C, 30mins | 4034.4 (bromobenzene) | --- | This work |
| Au-Pd alloy NP | DMF-H ₂ O, K ₂ CO ₃ 30 °C, 3h | 14.5 (bromobenzene) | --- | 17 |
| Au-Pd Nanostructure | H ₂ O, NaOH 25 °C, 1h | 162 (bromobenzene) | --- | 18 |
| Y₃Pd₂ | EtOH, K₂CO₃ 30 °C, 1h | 1432.6 (iodotoluene) | --- | This work |
| PDA/Pd NPs | DMF-H ₂ O, K ₂ CO ₃ RT, 2h | 85 (iodotoluene) | --- | 19 |
| WS ₂ /Pd NPs | EtOH-H ₂ O, K ₂ CO ₃ RT, 3 h | 1244 (iodotoluene) | --- | 20 |

Supplementary Table 6 Suzuki cross-coupling reactions of chlorobenzene with phenylboronic acid over Y_3Pd_2 .

| Entry | Aryl Halides | Arylboronic Acids | Product | Time (h) | Yield (%) |
|-------|---|---|--|----------|-----------|
| 1 |  |  |  | 24 | 7 |

Reaction conditions: Pd (40 mol% relative to organohalide); 0.5 mmol chlorobenzene, 0.8 mmol phenylboronic acid, 1.5 mmol K_2CO_3 , 5 mL solvent, 60 °C. An error analysis was performed for these data and the error range was determined to be $\pm 5\%$.

Supplementary Table 7 Characterization and activity of fresh and ball-milled Y₃Pd₂.

| Sample | S _{BET} (m ² g ⁻¹) | CO _{ads.} (ml g ⁻¹) | Exposed Pd by CO _{ads.} (10 ⁻⁶ mol g ⁻¹) | Exposed Pd by unit cell (10 ⁻⁶ mol g ⁻¹) | Reaction rate (mmol g ⁻¹ h ⁻¹) | TOFs by CO _{ads.} (h ⁻¹) | TOFs by unit cell. (h ⁻¹) |
|---|---|---|--|---|--|---|---|
| ^a Y ₃ Pd ₂ | 0.43 | 0.0198 | 0.9 | 1.8 | 3.04 | 3378 | 1670 |
| ^a Y ₃ Pd ₂ BM by heptane | 1.1 | 0.0617 | 2.7 | 4.6 | 6.41 | 2374 | 1393 |
| ^a Y ₃ Pd ₂ BM by ethanol | 3.2 | 0.1312 | 5.9 | 13.4 | 17.02 | 2934 | 1270 |
| ^b Y ₃ Pd ₂ | 0.43 | 0.0198 | 0.9 | 1.8 | 0.37 | 411 | 204 |

^a Reaction conditions: Pd (40 mol% relative to organohalide); 0.5 mmol iodobenzene, 0.8 mmol phenylboronic acid, 1.5 mmol K₂CO₃, 5mL solvent, 30 °C. ^b Pd (40 mol% relative to organohalide); 0.5 mmol bromobenzene, 0.8 mmol phenylboronic acid pinacol ester, 1.5 mmol K₂CO₃, 5 mL solvent, 60 °C. An error analysis was performed for these data and the error range was determined to be ±5%.

Supplementary Table 8 Bader charges of atoms on Y₃Pd₂(0001) surface before and after C₆H₅Br adsorption.

| | Pd | Y1 | Y2 | Y3 | C ₆ H ₅ Br |
|--|-------|-------|-------|-------|----------------------------------|
| Y ₃ Pd ₂ bulk | -1.88 | +1.39 | +1.19 | +1.23 | |
| Y ₃ Pd ₂ (0001) surface | -1.77 | +1.51 | +1.49 | +1.28 | |
| C ₆ H ₅ Br@Y ₃ Pd ₂ (0001) surface | -1.69 | +1.51 | +1.51 | +1.28 | -0.12 |

The Bader charges of atoms in Y₃Pd₂ bulk and The Bader charge of the C₆H₅Br molecule as a whole is also given. The results indicate a charge transfer of 0.12e⁻ from the Y₃Pd₂(0001) surface (mainly from the active Pd site) to the C₆H₅Br molecule.

Supplementary Table 9 Catalytic performance of Y₃Pd₂, Y₃Pd, Y₃Pd₄, YPd₃, Pd, Y₅Si₃ and Y powder.

| Catalyst | Surface area (m ² g ⁻¹) | Exposed Pd by unit cell (10 ⁻⁸ mol) | Reaction rate (mmol g ⁻¹ h ⁻¹) | Reaction rate (mmol m ⁻² h ⁻¹) | TOFs (h ⁻¹) |
|---|---|--|--|--|----------------------------|
| ^a Y ₃ Pd ₂ | 0.431 | 9.1 | 3.04 | 7.05 | 1670 |
| ^a YPd ₃ | 0.081 | 1.2 | 0.63 | 7.84 | 1562 |
| ^a Y ₃ Pd ₄ | 0.143 | 3.5 | 1.23 | 7.04 | 1291 |
| ^a Y ₃ Pd | 0.287 | 4.2 | 0.85 | 3.01 | 1578 |
| ^a Pd | 0.87 | 14 | 0.83 | 2.16 | 129 |
| ^b Y ₅ Si ₃ | 1.0 | -- | N.D. | N.D. | --- |
| ^c Y powder | 0.21 | -- | N.D. | N.D. | --- |

Reaction conditions: ^a Pd (40 mol% relative to organohalide); ^b Y₅Si₃ (50 mg); ^c Y powder (50 mg); 0.5 mmol iodobenzene, 0.8 mmol phenylboronic acid, 1.5 mmol K₂CO₃, 5mL solvent, 30 °C. An error analysis was performed for these data and the error range was determined to be ±5%.

Supplementary References

1. Park, I. et al. Atomic layer deposition of Y_2O_3 films using heteroleptic liquid (iPrCp)₂Y(iPr-amd) precursor, *J. Mater. Chem. C* **2**, 9240–9247 (2014).
2. Zhu, M. & Diao, G. Magnetically recyclable Pd nanoparticles immobilized on magnetic $Fe_3O_4@C$ nanocomposites: Preparation, characterization, and their catalytic activity toward Suzuki and Heck coupling reactions. *J. Phys. Chem. C* **115**, 24743–24749 (2011).
3. Zhang, A. et al. Homogeneous Pd nanoparticles produced in direct reactions: green synthesis, formation mechanism and catalysis properties. *J. Mater. Chem. A* **2**, 1369–1374 (2014).
4. Jiang, Y. et al. Simple synthesis of Pd– Fe_3O_4 heterodimer nanocrystals and their application as a magnetically recyclable catalyst for Suzuki cross-coupling reactions. *Phys. Chem. Chem. Phys.* **13**, 2512–2516 (2011).
5. Shylesh, S., Wang, L., Demeshko, S. & Thiel, W. R. Facile synthesis of mesoporous magnetic nanocomposites and their catalytic application in carbon–carbon coupling reactions. *ChemCatChem* **2**, 1543–1547 (2010).
6. Yuan, H., Liu, H., Zhang, B., Zhang, L., Wang, H. & Su, D. S. A Pd/CNT-SiC monolith as a robust catalyst for Suzuki coupling reactions. *Phys. Chem. Chem. Phys.* **16**, 11178–11181 (2014).
7. Zhang, P., Weng, Z., Guo, J. & Wang, C. Solution-dispersible, colloidal, conjugated porous polymer networks with entrapped palladium nanocrystals for heterogeneous catalysis of the Suzuki–Miyaura coupling reaction. *Chem. Mater.* **23**, 5243–5249 (2011).
8. Cargnello, M. et al. A versatile approach to the synthesis of functionalized thiol-protected palladium nanoparticles. *Chem. Mater.* **23**, 3961–3969 (2011).
9. Kim, E., Jeong, H. S. & Kim, B. M. Studies on the functionalization of MWNTs and their application as a recyclable catalyst for C–C bond coupling reactions. *Catal. Commun.* **46**, 71–74 (2014).
10. Roy, A. S. et al. Pd-grafted porous metal–organic framework material as an efficient and reusable heterogeneous catalyst for C–C coupling reactions in water. *Appl. Catal. A* **469**, 320–327 (2014).
11. Borhade, S. R. & Waghmode, S. B. Studies on Pd/NiFe₂O₄ catalyzed ligand-free Suzuki reaction in aqueous phase: synthesis of biaryls, terphenyls and polyaryls. *Beilstein J. Org. Chem.* **7**, 310–319 (2011).
12. Camp, J. E. et al. Glucose-derived palladium(0) nanoparticles as in situ-formed catalysts for Suzuki–Miyaura cross-coupling reactions in isopropanol. *ACS Sustainable Chem. Eng.* **2**, 500–505 (2014).

13. Song, H. Q., Zhu, Q., Zheng, X. & Chen, X. G. One-step synthesis of three-dimensional graphene/multiwalled carbon nanotubes/Pd composite hydrogels: an efficient recyclable catalyst for Suzuki coupling reactions. *J. Mater. Chem. A* **3**, 10368–10377 (2015).
14. Jiao, Z., Zhai, Z., Guo, X. & Guo, X. Y. Visible-light-driven photocatalytic Suzuki–miyaura coupling reaction on mott–schottky-type Pd/SiC catalyst. *J. Phys. Chem. C* **119**, 3238–3243 (2015).
15. Li, X. H., Baar, M., Blechert, S. & Antonietti, M. Facilitating room-temperature Suzuki coupling reaction with light: Mott-Schottky photocatalyst for C-C-coupling. *Sci. Rep.* **3**, 1743 (2013).
16. Zhang, S. et al. Visible-light-activated Suzuki–miyaura coupling reactions of aryl chlorides over the multifunctional Pd/Au/porous nanorods of CeO₂ catalysts. *ACS. Catal.* **5**, 6481–6488 (2015).
17. Xiao, Q. et al. Efficient photocatalytic Suzuki cross-coupling reactions on Au–Pd alloy nanoparticles under visible light irradiation. *Green Chem.* **16**, 4272–4285 (2014).
18. Wang, F. et al. Plasmonic harvesting of light energy for Suzuki coupling reactions. *J. Am. Chem. Soc.* **135**, 5588–5601 (2013).
19. Xie, A. et al. Polydopamine nanofilms as visible light-harvesting interfaces for palladium nanocrystal catalyzed coupling reactions. *Catal. Sci. Technol.* **6**, 1764–1771 (2016).
20. Raza, F., Yim, D., Park, J. H., Kim, H. I., Jeon, S. J. & Kim, J. H. Structuring Pd nanoparticles on 2H-WS₂ nanosheets induces excellent photocatalytic activity for cross-coupling reactions under visible light. *J. Am. Chem. Soc.* **139**, 14767–14774 (2017).